HOLISTIC DESIGN: OPTIMIZING MECHATRONIC SYSTEMS

USING MULTI OBJECTIVE OPTIMIZATION

by

Islam Adel Helmy Aly

A Thesis Presented to the Faculty of the
American University of Sharjah
College of Engineering
in Partial Fulfillment
of the Requirements
for the Degree of

Master of Science in
Mechatronics Engineering

Sharjah, United Arab Emirates

May 2015

Approval Signatures

We, the undersigned, approve the Master's Thesis of Islam Adel Helmy Aly

Thesis Title: Holistic Design: Optimizing Mechatronic Systems Using Multi Objective Optimization

Signature	**Date of Signature** (dd/mm/yyyy)
_____	_____
Dr. Lotfi Romdhane Professor Department of Mechanical Engineering Thesis Advisor	
_____	_____
Dr. Rached Dhaouadi Professor, Department of Electrical Engineering Thesis Committee Member	
_____	_____
Dr. Mohammad Nazzal Visiting Associate Professor, Department of Mechanical Engineering Thesis Committee Member	
_____	_____
Dr. Mamoun Abdel-Hafez Director Mechatronics Engineering Graduate Program	
_____	_____
Dr. Mohamed El-Tarhuni Associate Dean College of Engineering	
_____	_____
Dr. Leland Blank Dean College of Engineering	
_____	_____
Dr. Khaled Assaleh Director of Graduate Studies	

Acknowledgements

First of all, I would like to thank God, the most gracious most merciful for His unlimited gifts. I would like to thank my lovely parents and family for their endless support and guidance. Also, I would like to sincerely thank my brilliant mentor and advisor Dr. Lotfi Romdhane who taught, helped, and guided me patiently throughout my thesis. I would like to extend my gratitude to the committee members and the mechatronics engineering graduate program council members who reviewed my thesis for their constructive feedback. I also appreciate the tremendous support I got from the Department of Mechatronics Engineering at the American University of Sharjah for providing me with a graduate teaching assistantship for a semester. Finally, I would like to thank all my friends and colleagues for their support and encouragement.

... This thesis is dedicated to my beloved parents...

Abstract

This thesis aims to present an integrated approach to mechatronic systems design using heuristic optimization techniques. This integrated approach will consider the kinematics of the system, the dynamics, and the control simultaneously. The design methodology will be applied on a four-bar mechanism driven by a DC motor. First, we will present the classical design approach where we optimize the geometry of the mechanism to generate a given path. Then, this geometry is used to solve the dynamic problem where the characteristics of the motor and the mechanism inertia are considered. Afterwards, based on the designed system, the control system will be optimized. This sequential approach of design is not optimal due to the fact that the geometry is fixed when designing the dynamics and the plant is fixed when designing the controller. This led us to propose a holistic design approach where the kinematics, dynamics, motor selection, and control are considered simultaneously. The results from the holistic design approach are compared with the sequential approach to show the effectiveness of the proposed methodology.

Search Terms: Holistic design, Mechatronic systems, Four-Bar, Genetic Algorithm, Optimization

Table of Contents

List of Figures

List of Tables

Chapter 1: Introduction

Developing mechatronic systems requires knowledge in mechanical, electronic, control, and software engineering domains. These domains are interrelated and design decisions in one domain often affect others. Conventional sequential design methodologies do not consider the interactions and interrelations among these domains and a holistic approach of mechatronic systems design is demanded. However, challenges such as multidisciplinary modeling, simultaneous consideration of designs from different disciplines, and persistence of a sequential design process stand as a liability. Despite many research contributions aimed at providing a theoretical framework for the design, this goal has not been achieved [1].

1.1 Motivation

Mechatronic systems design is focused on recently as the research trend is moving towards automation [1, 2, 3]. In traditional design of mechatronic systems, the mechanical design is frozen before considering motor selection and the control design. This design approach does not consider the interaction between the mechanical, electronic, and control behaviors. As a result, the overall system design and performance is affected. This raises a need for a concurrent design approach that considers all different aspects of system design simultaneously.

1.2 Problem Statement

Using heuristic optimization techniques in design is popular in the literature. Several researchers optimized the kinematics of the system, such as the geometry in path synthesis [4, 5, 6]. Some researchers optimized the mechanical properties, such as the geometry and the inertia while taking into account the motor parameters [7, 8]. Other researchers looked into using heuristic techniques to get the optimal tuning of control gains [9]. But these cited works fell short from considering the mechanical, electronic, and the control problems, simultaneously, in design. Recently, some preliminary works presented methodologies to optimize all the aspects of a closed-loop controlled system. This type of problem is of a multidisciplinary nature, with parameters and criteria of different physical natures. To be able to solve this holistic design problem, a multi-objective optimization technique needs to be formulated dealing with the multi-physics nature of mechatronic systems, where the mechanical system, the actuator, and control are to be considered simultaneously.

1.3 Contributions

This work proposes a holistic design methodology for mechatronic systems that considers the mechanical system design, actuator selection, and control system design, simultaneously. This design methodology will alter the plant and the controller designs.

1.4 Thesis Outline

This thesis is organized as follows: a detailed literature review about design using heuristic techniques will be presented in Chapter 2. Chapter 3 will focus on mechanism synthesis, coupled dynamics and motor selection, and control system optimization. In Chapter 4, the design problem is formulated and a comparison between the proposed design approach and the conventional sequential design is made and the multi-objective optimization problem is formulated. Chapter 5 concludes the work outcomes and proposes future work.

Chapter 2: Related Work

2.1 Literature Review

Different heuristic optimization techniques can be used to solve problems of a complex nature. However, genetic algorithms have strength in design due to the fact that they are flexible, result in robust and stable algorithms, simple, and can be used with continuous and discrete variables. They can also handle the complexity of large problems by their ability to work with many variables, simultaneously, in a search domain of a complicated structure [10]. They, as well, have a powerful search capability [9]. However, they have to be designed carefully to ensure diversity.

A four-bar mechanism driven by a DC motor will be considered as the design case in this thesis. Mechanisms form the skeleton of machines and are widely used in industry. Four-bar mechanisms are used in a variety of applications. In the automotive industry, watt's linkage is used in car suspensions and piston cylinder slider crank four-bar mechanisms are used in car engines. In the oil and gas industry, a pump jack four-bar mechanism is used to pump up oil when the underground pressure is not enough for the oil to reach the surface. In aerospace, four-bar mechanisms are used in wing leading edge movement to increase wing camber at low speeds, flight control systems of fighter jets by utilizing a series of four-bar mechanisms, tail elevator control by using two four-bar mechanisms connected by a cable, and propeller blade pitch control of a helicopter [11].

Some researchers concentrated on the path synthesis of mechanisms and used different optimization techniques to solve for the geometry that will yield the desired path [4, 5, 10]. Others considered the coupled four-bar mechanism and aimed to optimize the link dimensions that minimize the path error and at the same time optimize the dynamic behavior, i.e., minimum torque and torque fluctuations, by minimizing the current and the current variation [8]. Some authors [7] minimized motor torque as well as the velocity fluctuation of the system by considering the inertia of the system and different motors to run the system adding a discrete variable into the optimization problem.

Others [9] concentrated on control such as using differential evolution optimization to tune PID gains for given specifications. Another paper [12] used an

adaptive micro-genetic algorithm to tune the controller gains relying on the frequency response gain phase margin method.

2.2 Genetic Algorithms

The genetic algorithm (GA) is an optimization and search technique based on the principles of genetics and natural selection. A GA allows a population composed of many individuals to evolve under specified selection rules to a state that maximizes the "fitness" (i.e., minimizes the cost function) [13].

The following are some of the advantages of GAs:

• Optimization with continuous or discrete variables

• No need for derivative information

• Simultaneous search from a wide sampling of the cost surface

• Possibility of dealing with a large number of variables

• Well-suited for parallel computers

• Optimization of extremely complex cost surfaces (they can jump out of a local minimum)

• The results are a list of optimum solutions, not just a single solution

• Optimization with numerically generated data, experimental data, or analytical functions

The Genetic algorithm starts with a population of chromosomes with each chromosome having a sequence of data. In our design, a chromosome is a design vector and the data in the chromosome represents the design variables. Some of these chromosomes are subjected to mutation. The fraction of mutation is a choice left to the designer. Then crossover between chromosomes takes place, just like in nature. The front part of one chromosome and the back part of the other fuse together and new chromosomes are generated. Some chromosomes may slip without crossover. The fraction of crossover is a choice left to the designer. Now that a population of modified chromosomes through mutation and crossover is obtained, the next step is the genotype to phenotype transition; that is, the chromosome determines whether the individual is a person, a computer program, or so on. The chromosome resembles the genotype and the chromosome data is interpreted to a phenotype. This interpretation

generates individuals that have different fitness values because they have varying chromosomal composition. The criterion for fitness is selected by the designer based on the application. The fitness value is translated to a probability of survival to the next generation. The choice of how the individual fitness is evaluated, and how the fitness yields a probability is all left to the designer. The probabilities are then used for selection and the phenotypes produce genotypes (a new set of chromosomes). That completes the loop and a new generation starts [14].

A flow chart of the genetic algorithm (GA) and the multi-objective genetic algorithm (MOGA) is illustrated in Figure 1. In the case of the multi-objective GA, the outer loop represents one evolutionary period and the inner loop represents one GA generation. In a mono-objective GA, the dashed boxes and loop are not there [8]. The first step is the generation of the initial population (X_0). For each individual in the population, the objective function is evaluated. Then by selection, crossover, and mutation, the population is modified and the individuals are evaluated based on the objective function. The population for the new generation denoted with "i" is obtained and the loop continues till the maximum number of generations (N) is reached. For the multi-objective GA, the non-dominated solutions obtained in the evolutionary period are added to the elitist Paretian population (X_{Par}) and then filtered to obtain a non-dominated population. These non-dominated individuals provide solutions that are not dominated in at least one of the objective functions.

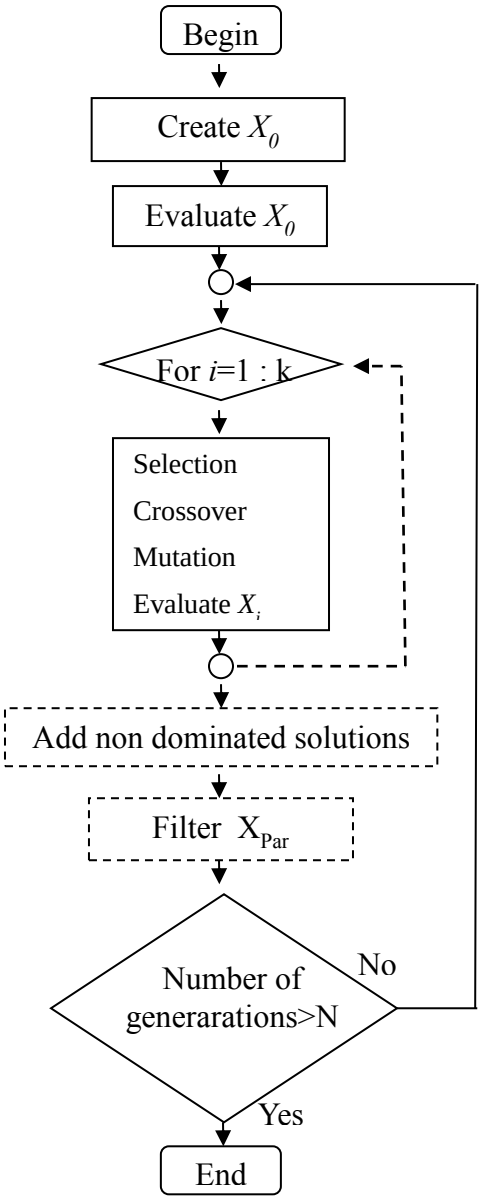

Figure 1: GA and MOGA Flow Chart [8]

Chapter 3: System Analysis

3.1 Mechanism Synthesis

3.1.1 Introduction.

In most engineering design practices, a combination of synthesis and analysis is involved. However, a machine has to be synthesized into existence before analysis can be done [15]. Andre Marie Ampere defined kinematics as "the study of the motion of mechanisms and methods of creating them." The second part of Ampere's definition may be paraphrased in two ways:

1) The study of methods of creating a given motion by means of mechanisms
2) The study of methods of creating mechanisms having a given motion

In either version, the motion is given and the mechanism is to be found. Thus, kinematic synthesis deals with the systematic design of mechanisms for a given performance [16].

Synthesis can be classified into two categories: type and dimensional synthesis. Type synthesis studies what type of mechanism is suitable for the required performance. Dimensional synthesis is determining the significant dimensions and the starting position of a mechanism for a desired motion and prescribed performance [16].

The path generation of a mechanism can be solved for analytically, numerically, and graphically [15]. However, formulating dimensional synthesis as an optimization problem increases the number of precision points that can be solved for and reduces the tracking error [17].

3.1.2 Mechanism.

A mechanism is an assembly of links which has at least one degree of freedom, in which the links will have relative motions.

3.1.2.1 A four-bar mechanism.

One of the most common and most useful of all mechanisms is the four-bar linkage [18]. A four-bar linkage is shown in Figure 2. It is a pin jointed mechanism that generates a one degree of freedom controlled motion. It is composed of four

links: the ground link, the crank, the coupler, and the follower. The ground link is a fixed link, the crank is the link that drives the mechanism as the actuator is connected to its pin joint, and the coupler is usually the link of interest as it generates complex motion. A four-bar mechanism is shown below where L_1 represents the ground link, L_2 represents the crank, L_3 represents the coupler, and L_4 represents the follower pin-to-pin lengths.

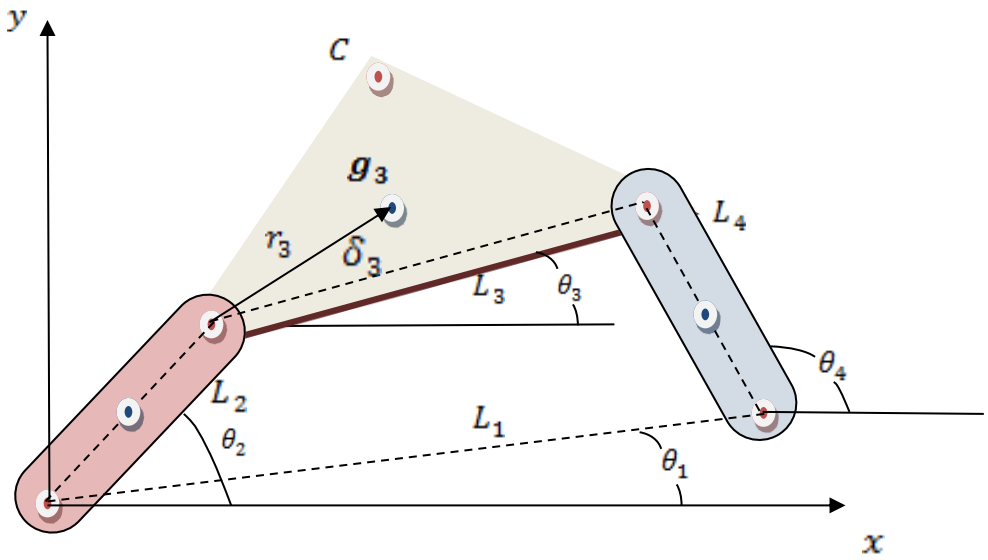

Figure 2: Four-Bar Mechanism

3.1.2.2 Grashof condition.

The Grashof condition is a relationship that predicts the rotation behavior of a four-bar linkage's inversions based on the link lengths [15]. If the summation of the shortest and the longest links is less than or equal to the other two links, then the linkage is Grashof and at least one link is capable of achieving a complete revolution. The inequality is shown in equation (1).

$$S + L \leq P + Q \tag{1}$$

where S is the shortest length, L is the longest length, and P and Q are the other two lengths of the mechanism.

If the linkage fails to satisfy the inequality, then the linkage is non-Grashof and no link can generate a full revolution. The motions yielded by a four-bar linkage depend on the Grashof condition and the inversion chosen. Given that the linkage is Grashof, the same linkage can generate three different motions depending on what link is made the ground link. If either of the links adjacent to the shortest link is made

the ground, the shortest link will fully rotate and the follower will oscillate. This mechanism is referred to as a crank-rocker. If the shortest link is made the ground, all links will fully rotate; this mechanism is referred to as a double-crank. If the link opposite to the shortest link is made the ground, only the coupler will fully rotate. This mechanism is called a double-rocker.

3.1.2.3 Position analysis.

One approach to position analysis is to create a vector loop by using position vectors to represent the links [19]. These vectors form a loop that closes in on itself and equates to zero. Given certain link lengths and input angle θ_2, it is desired to solve for the unknown angles $\theta_3$and θ_4. Figure 3 shows a four-bar linkage in which the links are represented as position vectors.

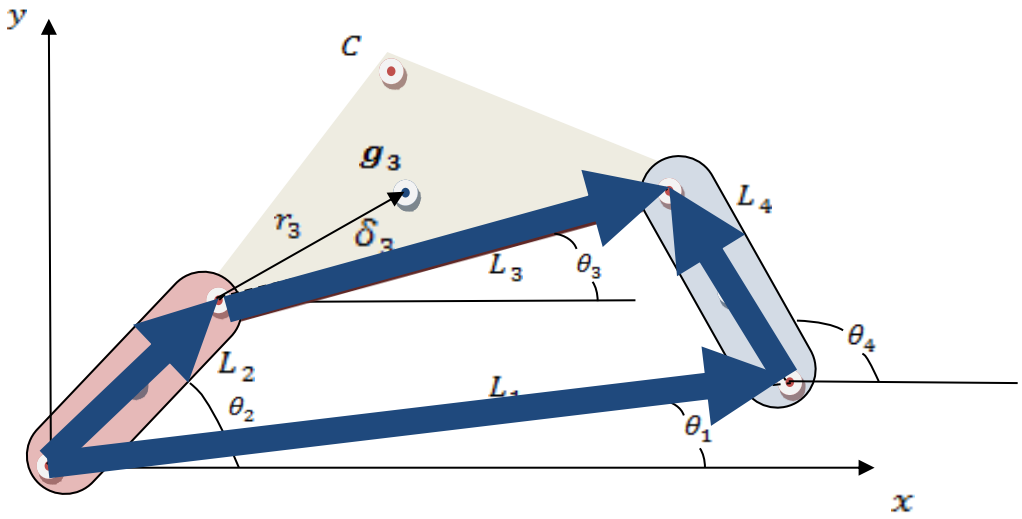

Figure 3: Vector Loop Closure

Starting with the vector loop closure equation:

$$\vec{\boldsymbol{L}}_{\boldsymbol{2}} + \vec{\boldsymbol{L}}_{\boldsymbol{3}} = \vec{\boldsymbol{L}}_{\boldsymbol{4}} + \vec{\boldsymbol{L}}_{\boldsymbol{1}} \tag{2}$$

Then, by substituting the complex notation for each position vector:

$$L_2 e^{j\theta_2} + L_3 e^{j\theta_3} = L_4 e^{j\theta_4} + L_1 e^{j\theta_1} \tag{3}$$

Substituting the Euler equivalents for the exponential terms:

$$\begin{aligned} L_2(\cos(\theta_2) + \mathrm{j}\,\sin(\theta_2)) + L_3(\cos(\theta_3) + \mathrm{j}\,\sin(\theta_3)) \\ = L_4(\cos(\theta_4) + \mathrm{j}\,\sin(\theta_4)) + L_1(\cos(\theta_1) + \mathrm{j}\,\sin(\theta_1)) \end{aligned} \tag{4}$$

By separating the resulting vector equation into two scalar equations, the two unknowns $\theta_3$and θ_4 can be solved for:

$$L_2\cos(\theta_2) + L_3\cos(\theta_3) = L_4\cos(\theta_4) + L_1\cos(\theta_1) \quad (5)$$

$$L_2\sin(\theta_2) + L_3\sin(\theta_3) = L_4\sin(\theta_4) + L_1\sin(\theta_1) \quad (6)$$

Squaring both sides of the equations, grouping $\theta_3$terms and using the identity $\sin^2(\theta) + \cos^2(\theta) = 1$, $\theta_3$gets eliminated and the equation can be solved for θ_4:

$$\begin{aligned} {L_3}^2 = {L_1}^2 + {L_2}^2 + {L_4}^2 + 2L_1L_4(&\cos(\theta_1)\cos(\theta_4) + \sin(\theta_1)\sin(\theta_4)) \\ &- 2L_1L_2\cos(\theta_1 - \theta_2) - 2L_2L_4(\cos(\theta_2)\cos(\theta_4) \\ &+ \sin(\theta_2)\sin(\theta_4)) \end{aligned} \quad (7)$$

Taking $\sin(\theta_4)$ and $\cos(\theta_4)$ as common factors to obtain an explicit form of θ_4 :

$$\begin{aligned} {L_1}^2 + {L_2}^2 + {L_4}^2 - {L_3}^2 &- 2L_1L_2\cos(\theta_1 - \theta_2) \\ &+ (2L_1L_4\cos(\theta_1) - 2L_2L_4\cos(\theta_2))\cos(\theta_4) \\ &+ (2L_1L_4\sin(\theta_1) - 2L_2L_4\sin(\theta_2))\sin(\theta_4) = 0 \end{aligned} \quad (8)$$

The equation in (8) can be rewritten as in (9).

$$A\cos(\theta_4) + B\sin(\theta_4) + C = 0 \quad (9)$$

where,

$$A = 2L_1L_4\cos(\theta_1) - 2L_2L_4\cos(\theta_2) \quad (10)$$

$$B = 2L_1L_4\sin(\theta_1) - 2L_2L_4\sin(\theta_2) \quad (11)$$

$$C = {L_1}^2 + {L_2}^2 + {L_4}^2 - {L_3}^2 - 2L_1L_2\cos(\theta_1 - \theta_2) \quad (12)$$

Substituting the half angle identities for $\cos(\theta_4)$ and$\sin(\theta_4)$, shown in (13, 14), to solve for θ_4:

$$\cos(\theta_4) = \frac{1 - tan^2\left(\frac{\theta_4}{2}\right)}{1 + tan^2\left(\frac{\theta_4}{2}\right)} \quad (13)$$

$$\sin(\theta_4) = \frac{2\tan\left(\frac{\theta_4}{2}\right)}{1 + tan^2\left(\frac{\theta_4}{2}\right)} \quad (14)$$

After simplifying the equation becomes:

$$(C - A)tan^2\left(\frac{\theta_4}{2}\right) + 2B\tan\left(\frac{\theta_4}{2}\right) + (C + A) = 0 \quad (15)$$

Solving the quadratic equation (15) yields:

$$\theta_{4_{1,2}} = 2tan^{-1}\left(\frac{-B \pm \sqrt{B^2 + A^2 - C^2}}{C - A}\right) \tag{16}$$

There are two solutions for θ_4, obtained from $\pm$ before the radical for the open and crossed linkage, respectively.

Substituting θ_4 back in equation (5) and simplifying $\theta_3$becomes:

$$\theta_3 = tan^{-1}\left(\frac{L_4 \sin(\theta_4) + L_1 \sin(\theta_1) - L_2 \sin(\theta_2)}{L_4\cos(\theta_4) + L_1\cos(\theta_1) - L_2\cos(\theta_2)}\right) \tag{17}$$

3.1.3 Coupler point.

A coupler is the most interesting link in a linkage due to its complex motion. In dimensional synthesis of a mechanism a number of precision points (desired points) are to be traced by the coupler point. In four-bar linkage synthesis the dimensions of the links (L_1, L_2, L_3, L_4) and the coupler point location (r_{cx}, r_{cy}) are to be designed such that the generated path by this mechanism traces the precision points. The smaller the error between the precision points and the designed mechanism generated points, the better the design. The generated points or evaluated points are derived in this section.

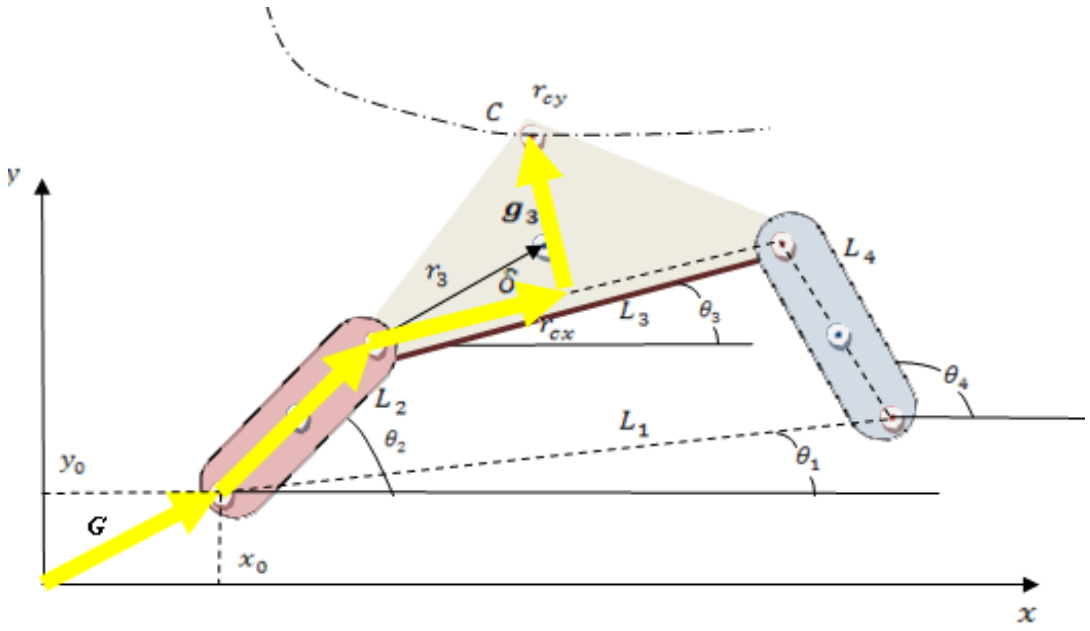

Figure 4: Coupler Point Mapping

Considering the relative position of the linkage to a global reference frame gives more flexibility to the generated coupler curve and reduces the tracing error as

the orientation of the generated points is varied to match with the precision points. The position of the coupler point in the global reference frame is shown in Figure 4 and the vector equation is shown in (18).

$$\vec{\boldsymbol{C}} = \vec{\boldsymbol{G}} + \vec{\boldsymbol{L}}_{\boldsymbol{2}} + \vec{\boldsymbol{r}}_{\boldsymbol{cx}} + \vec{\boldsymbol{r}}_{\boldsymbol{cy}} \tag{18}$$

The vector equation can be separated into the following two scalar equations (19, 20) that represent the coupler point coordinates in the global reference frame:

$$C_{xr} = x_0 + L_2\cos(\theta_2) + r_{cx}\cos(\theta_3) - r_{cy}\sin(\theta_3) \tag{19}$$

$$C_{yr} = y_0 + L_2\sin(\theta_2) + r_{cx}\sin(\theta_3) + r_{cy}\cos(\theta_3) \tag{20}$$

3.1.4 Objective function.

The use of heuristic techniques in path synthesis increases the number of precision points that can be solved for and reduces the tracking error [17]. The design of the geometry of the mechanism to track a desired path accurately is the goal of this problem. The objective function is formulated here as the sum of the squared errors between each desired and obtained point.

The desired location of the points is written as

$$C_d^i = \begin{bmatrix} C_{xd}^i \\ C_{yd}^i \end{bmatrix} \tag{21}$$

And the generated coupler points are shown in the previous section.

$$C_g^i = \begin{bmatrix} C_{xr}^i \\ C_{yr}^i \end{bmatrix} \tag{22}$$

The objective function to be minimized is given by (23).

$$\mathrm{f}_1\text{: min}\left(\sum_{i=1}^{n}\left(C_{xd}^i - C_{xr}^i\right)^2 + \left(C_{yd}^i - C_{yr}^i\right)^2\right)^{1/2} \tag{23}$$

3.1.4.1 Design vector.

The design vector for the genetic algorithm is given by:

$$X = [\, x_0,\, y_0, \theta_1,\, L_1,\, L_2,\, L_3,\, L_4,\, r_{cx}, r_{cy}, \theta_2\,] \tag{24}$$

The design vector is made of 10 variables: the orientation of the ground link in the global frame, the link lengths, the position of the coupler point, and the crank angle of the first point.

3.1.4.2 Constraints.

The optimization is subject to some constraints that have to be satisfied by the individuals in each generation. The two constraints for the synthesis problem are presented in equations (25) and (26):

The Grashoff condition:

$$g_1(x): L_1 + L_2 \ < \ L_3 + L_4 \tag{25}$$

The linkage inversion considered here is the crank-rocker Grashof mechanism in which the ground link is adjacent to the shortest link.

Each design variable is bound in a range:

$$g_2(x): x_i \in [\, x_{i\,min},\ x_{i\,max}] \tag{26}$$

The individuals generated in each population have to satisfy these two constraints.

3.1.5 Example problem.

The objective is to synthesize a mechanism that will trace 18 precision points with prescribed timing. This problem is solved as a case study in [5].

The desired points and prescribed input crank angles are shown below.

C_d^i = [(0.5,1.1) ; (0.4,1.1); (0.3,1.1) ; (0.2,1.0) ; (0.1,0.9) ; (0.005,0.75) ; (0.02,0.6) ; (0.0,0.5) ; (0.0,0.4) ; (0.03,0.3) ; (0.1,0.25) ; (0.15,0.2) ; (0.2,0.3) ; (0.3,0.4) ;(0.4,0.5) ; (0.5,0.7) ; (0.6,0.9) ; (0.6,1.0)]

$\theta_2{}^i = [\, \theta_2{}^1, \theta_2{}^1 + 20i\,]$ {i = 1, 2, …, 17}

3.1.5.1 Genetic algorithm.

To start with, the genetic algorithm toolbox in Matlab is used for implementation. Two constraints are set that have to be satisfied by the individuals in each generation. Bounded ranges are chosen for the design variables. These bounds are shown below.

$$-1 < x_0,\ y_0 < 1$$

$$0 < \theta_1, \theta_2 < 2\pi$$

$$0.05 < L_i < 1$$

$$-1 < r_{cx}, r_{cy} < 1$$

The individuals also have to satisfy the Grashof condition. The individuals were arranged to yield a crank-rocker mechanism. The ground link is made the longest link and the crank the shortest.

The fitness scaling function is the function used to convert the raw fitness scores to values suitable for the selection process. A good fitness scaling function considers both fitness and diversity. The scaling function used is based on the rank of the individual in the population. An individual with rank r has a scaled score of $1/\sqrt{r}$ [20]. Rank scaling gives high expectations for highly ranked individuals and low expectations for individuals with low fitness, yet individuals with low fitness have a probability of being selected to the next generation, hence increasing the diversity of the population.

The selection function specifies the choice of parents for the next generation. The selection function can be stochastic uniform based on stochastic universal sampling [21], in which the scaled scores of the individuals in the current population make up a line with each individual having a proportional section of the line. The algorithm allocates a parent from the section it lands on randomly. The remainder function chooses parts based on the integer part of the individuals scaled values [20]. There is also roulette selection, in which the parents are selected by simulating a roulette wheel. The individuals' expectation is translated into an area on the roulette wheel. The tournament selection function creates sized tournaments between random individuals and the best in each tournament qualifies to be a parent for the next generation.

A Monte Carlo study [22] was done to check which of these selection functions is more suitable to the problem. The results of GA using different selection functions computed over 10 iterations are shown in Figure 5, where functions 1, 2, 3, and 4 are the stochastic uniform, remainder, roulette, and tournament, respectively.

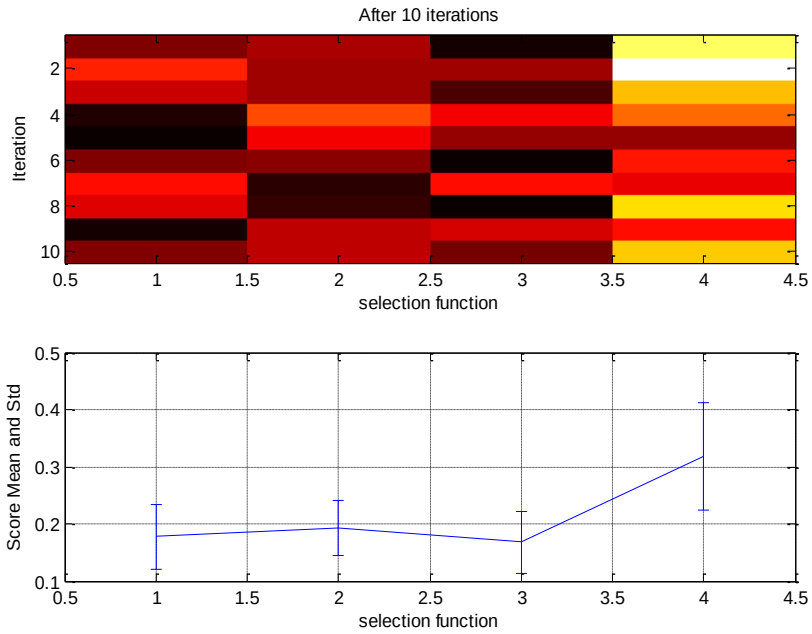

Figure 5: Choosing a GA Selection Function - Synthesis

In Figure 5, the top portion represents a color map of the minimized objective function values over the 10 iterations; the darker the color the smaller the value. The lower portion shows the mean and standard deviations of the values obtained over the 10 iterations. It can be noticed that the roulette and the stochastic uniform functions yield the lowest mean and standard deviation and hence are more suitable to be used as a selection function than the other methods.

After selecting the parents for the next generation, we must select the portion of the offspring due to crossover and the portion due to mutation and the used functions. The mutation function used is adaptive feasible; the function randomly generates directions adaptive with the last generation and with a step size that satisfies the bounds and constraints. The crossover function choice is going to be from the intermediate, heuristic, and arithmetic crossover functions. The intermediate function produces children using equation (27).

$$child = parent1 + rand * ratio * (parent2 - parent1) \qquad (27)$$

It produces children that are the weighted average of their parents; the weights can be specified by the *ratio* in (27). If the ratio is less than one, then the child is in the hypercube defined by the parents; otherwise the children might lie outside the hypercube [20]. A random number (*rand*) from zero to one is multiplied by the difference between the parents.

The heuristic function produces children that lie on a line containing the two parents a small distance away from the fitter parent. If parent1 is the parent with better fitness, then the child is produced as in equation (28),

$$child = parent2 + ratio * (parent1 - parent2) \quad (28)$$

where the *ratio* specifies how far the child is from the better parent. The arithmetic function produces a child with genes that are the arithmetic mean of the parents' genes.

A Monte Carlo study was done to select a crossover function suitable for this problem shown in Figure 6, where functions 1, 2, and 3 are the intermediate, heuristic, and arithmetic, respectively.

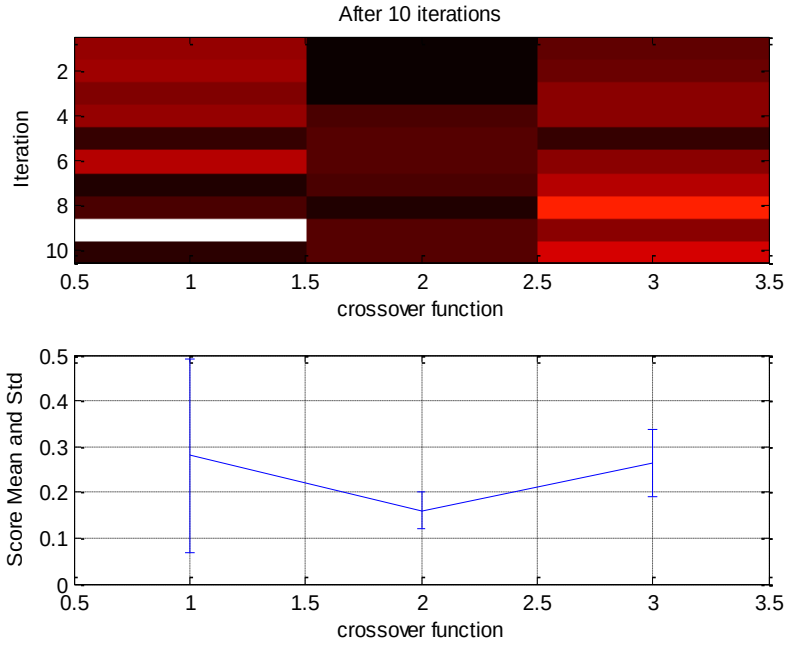

Figure 6: Choosing a GA Crossover Function - Synthesis

A GA is simulated for 10 iterations using each of the crossover functions, and from the obtained objective function values, the heuristic crossover function yields the lowest mean and standard deviation. Now that the heuristic crossover function is selected, the heuristic crossover ratio and the crossover fraction of the generated offspring are chosen in the same manner.

By running some Monte Carlo studies, the options used to run the GA are selected and shown in Table 1.

Table 1: Synthesis GA Options

Option	Choice
Population size	100
Generations	200
Elite count	4
Crossover fraction	0.52
Scaling function	Rank
Selection function	Stochastic uniform
Mutation function	Adaptive feasible
Crossover function	Heuristic

Running the GA, the best fit individual after 200 generations and the average of the generations are shown in Figure 7 .

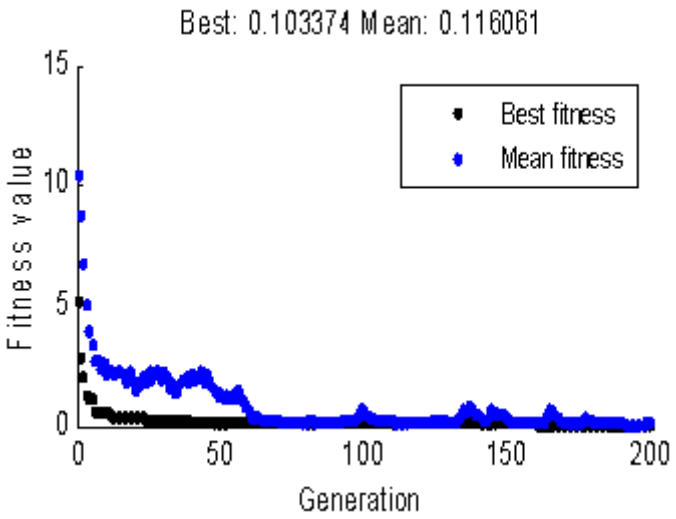

Figure 7: Synthesis GA Analysis

3.1.5.2 Results.

The resulting design vector and the objective function value representing the square root of the sum of square errors are shown in Table 2.

Table 2: Four-Bar Mechanism Synthesis Using GA

Mechanism Design Vector (X)										
x_0 (m)	y_0 (m)	θ_1 (rad)	L_1 (m)	L_2 (m)	L_3 (m)	L_4 (m)	r_{cx} (m)	r_{cy} (m)	$\theta_{2,0}$ (m)	error
0.235	0.2735	0.2061	0.9196	0.4322	0.7565	0.617	0.3217	0.2906	1.1533	0.103

Computing position analysis and coupler point path generation, Figure 8 shows the desired path and the designed mechanism-generated path.

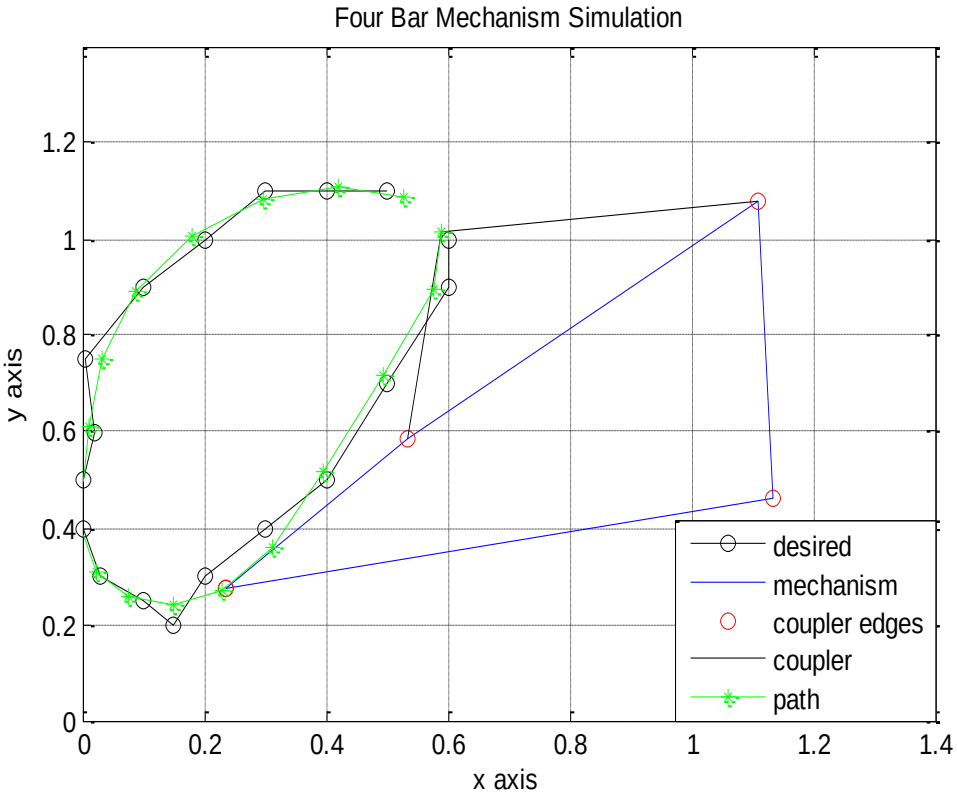

Figure 8: GA Four-Bar Simulation

Since the GA gets a solution near the global minimum, a hybrid function can be considered in which a local minimization function, fmincon, runs after the GA terminates to reach the closest minima. Computing the hybrid function, the error value reduces as shown in Table 3 along with the design vector.

Table 3: Four-Bar Mechanism Synthesis Using Hybrid GA

Mechanism Design Vector (X)										
x_0 (m)	y_0 (m)	θ_1 (rad)	L_1 (m)	L_2 (m)	L_3 (m)	L_4 (m)	r_{cx} (m)	r_{cy} (m)	$\theta_{2,0}$ (m)	error
0.2553	0.1868	0.3078	1.0	0.4261	0.8807	0.5764	0.3639	0.3621	1.1708	0.0998

The solution obtained in Figure 9 is compared with the solutions presented in the case study in [5] for the same desired path and the results are presented in Figure 10.

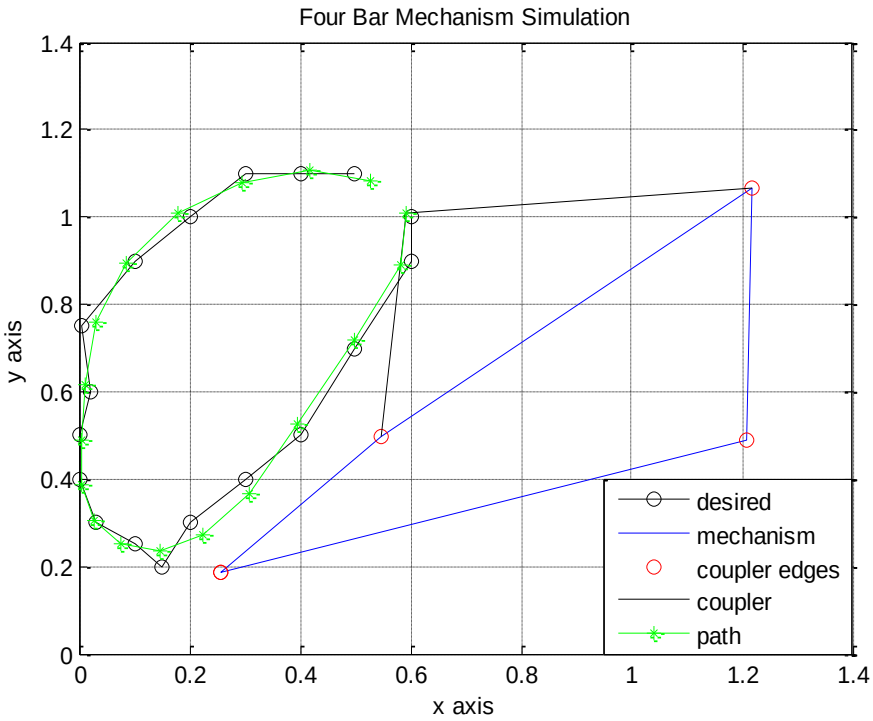

Figure 9: Hybrid GA Four-Bar Simulation

Figure 10 shows the generated path of the synthesized geometric parameters obtained in different articles along with the desired path. It can be noticed in Table 4 that the mean error obtained is smaller than the error obtained in the other articles.

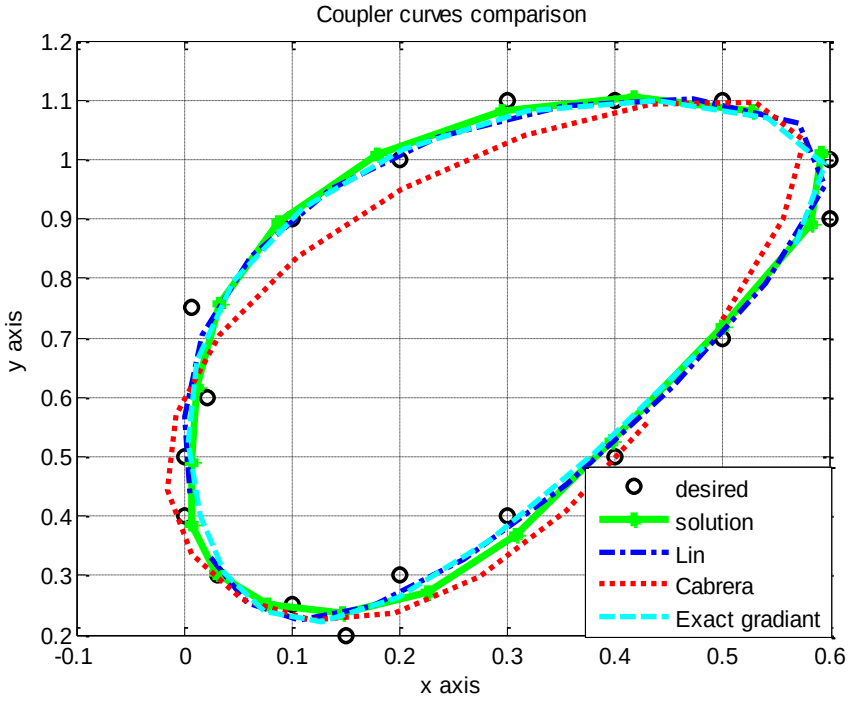

Figure 10: Coupler Curves Comparison

The sum of the square errors is shown in Table 4.

Table 4: Fitness Value Comparison

	Synthesized results			
	Solution	Lin	Cabrera	Exact gradiant
$fval^2$	1.00×10^{-2}	1.08×10^{-2} [5]	3.48×10^{-2}[23]	1.09×10^{-2}[24]

3.2 Dynamics

3.2.1 Introduction.

In machine design, only taking the geometry and the kinematics into consideration is oversimplifying the problem. After studying the geometry and motion of a machine comes the study of the forces required to produce the motion or the effect of the applied forces on motion [18]. The dynamics problem is classified into subclasses based on what is known and what is unknown. The forward dynamics subclass solves the problem in which all loads exerted on the system are known and the motion that would result from the application of those forces and torques is to be determined. The inverse dynamics subclass solves the problem in which the imposed accelerations, velocities, and displacements are known and the forces and the torques required to provide the desired motions are solved for [15].

Dynamic systems can be simplified into models of point masses. However, for a rigid body model to be equivalent to the original body, the mass, the center of gravity location, and the mass moment of inertia of the model must be equal that of the original body [15].

3.2.2 Rigid body model.

The shape and the properties of the links are considered in this section. The links are octagonal in shape and are considered to be made of a homogeneous material. The geometric parameters of the links affect the dynamic behavior of the links tremendously. These parameters modify in a direct way the mass of the link, the center of mass location, and the inertia, respectively. The reason behind choosing an octagonal shape for the link is that by modifying the octagon dimensions, the center of mass angle can move in the interval from [0,±π], hence providing more diversity to the search domain making it richer in solutions than the rectangular shape of links in which the center of mass angle can only be 0 or ±π [25]. The relationship between the

dimensions of the octagonal link, specified by $l_i, b_i, c_i, d_i, e_i, f_i, g_i, h_i, i_i, j_i, k_i$ and the mass, the center of mass location, and the inertia are derived in this section [26].

The geometric parameters of link i are shown in Figure 11. The following is to be considered in the derivation [26].

- The coordinate origin is placed at the C hole as shown above
- The links can move in the x-y plane only
- There is a shaft in the B hole of the crank and follower links (connection to the coupler). A cylindrical support is placed in the C hole of the crank and follower links (connection to ground)
- Links and the cylindrical supports are made of aluminum $\rho_{al} = 2710\ kg\ m^{-3}$ and shafts are made of steel $\rho_{st} = 7840\ kg\ m^{-3}$
- The radius of the B hole is $r_B = 3.175 \times 10^{-3} m$, the radius of the C hole is $r_{i_{2,4}} = 0.006\ m$, the radius of the cylindrical supports is $r_{csC} = 19.05 \times 10^{-3} m$, and the length of the cylindrical support is $L_{cs} = 0.01\ m$
- Links are divided into simple geometries, A, B, C, D, E, F, G, H, and I, to compute the inertia [27]
- The mass of the link is assumed to be concentrated at the center of mass location of the link

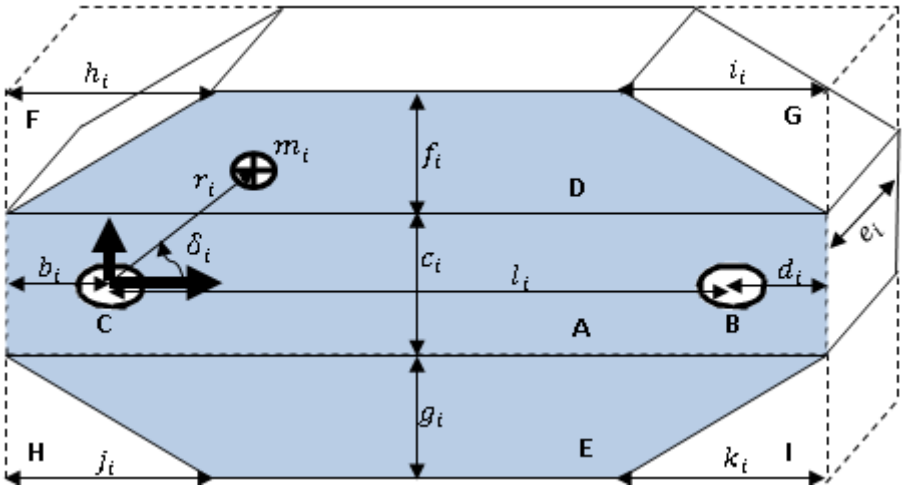

Figure 11: Link Schematic

The mass, the center of mass location, and the inertia of the links are obtained in terms of the geometric parameters in the following subsections.

3.2.2.1 Mass.

The masses of the links are composed of the masses of the divided portions of the link,m_{S_i}, and the masses of the supports, m_{shaftB_i}, m_{csC_i}.

$$m_2 = m_{S_2} + m_{shaftB_2} + m_{csC_2} \tag{29}$$

$$m_3 = m_{S_3} \tag{30}$$

$$m_4 = m_{S_4} + m_{shaftB_4} + m_{csC_4} \tag{31}$$

The sum of the masses of the simplified portions of a link is shown in equation (32).

$$m_{S_i} = m_{A_i} - m_{B_i} - m_{C_i} + m_{D_i} + m_{E_i} - m_{F_i} - m_{G_i} - m_{H_i} - m_{I_i} \tag{32}$$

The masses of the portions are shown in equations (33-41).

$$m_{A_i} = \rho_{al}((l_i + b_i + d_i) \times c_i \times e_i) \tag{33}$$

$$m_{B_i} = \rho_{al}(\pi {r_B}^2 \times e_i) \tag{34}$$

$$m_{C_i} = \rho_{al}(\pi {r_i}^2 \times e_i) \tag{35}$$

$$m_{D_i} = \rho_{al}((l_i + b_i + d_i) \times f_i \times e_i) \tag{36}$$

$$m_{E_i} = \rho_{al}((l_i + b_i + d_i) \times g_i \times e_i) \tag{37}$$

$$m_{F_i} = \frac{1}{2}\rho_{al}(h_i \times f_i \times e_i) \tag{38}$$

$$m_{G_i} = \frac{1}{2}\rho_{al}(i_i \times f_i \times e_i) \tag{39}$$

$$m_{H_i} = \frac{1}{2}\rho_{al}(j_i \times g_i \times e_i) \tag{40}$$

$$m_{I_i} = \frac{1}{2}\rho_{al}(k_i \times g_i \times e_i) \tag{41}$$

The masses of the shafts and cylindrical supports are shown in equations (42-44).

$$m_{shaftB_2} = \rho_{st} \times \pi {r_B}^2 \times (e_2 + e_3) \tag{42}$$

$$m_{shaftB_4} = \rho_{st} \times \pi {r_B}^2 \times (e_4 + e_3) \tag{43}$$

$$m_{csC_{i_{2,4}}} = \rho_{al} \times (\pi {r_{csC}}^2 - \pi {r_i}^2) \times L_{cs} \tag{44}$$

3.2.2.2 Center of mass.

The center of mass location for the i^{th} link is determined by the center of mass length and angle shown in equations (45, 46). The x-y coordinates of the mass center of the link portions and supports make up the total mass center coordinates x_{CM_i}, y_{CM_i}.

$$r_i = \sqrt{{x_{CM_i}}^2 + {y_{CM_i}}^2} \tag{45}$$

$$\delta_i = \tan^{-1}\left(\frac{y_{CM_i}}{x_{CM_i}}\right) \tag{46}$$

The center of mass coordinates of a link are the sum of the moments of the simplified portions of a link and the moment of the support around the x-y frame over the mass of the link as shown in equations (47-52) for the crank, coupler, and follower.

$$x_{CM_2} = x_{S_2} + \frac{x_{shaftB_2} m_{shaftB_2}}{m_2} \tag{47}$$

$$y_{CM_2} = y_{S_2} + \frac{y_{shaftB_2} m_{shaftB_2}}{m_2} \tag{48}$$

$$x_{CM_3} = x_{S_3} \tag{49}$$

$$y_{CM_3} = y_{S_3} \tag{50}$$

$$x_{CM_4} = x_{S_4} + \frac{x_{shaftB_4} m_{shaftB_4}}{m_4} \tag{51}$$

$$y_{CM_4} = y_{S_4} + \frac{y_{shaftB_4} m_{shaftB_4}}{m_4} \tag{52}$$

where

$$x_{S_i} = \frac{x_{A_i} m_{A_i} - x_{B_i} m_{B_i} - x_{C_i} m_{C_i} + x_{D_i} m_{D_i} + x_{E_i} m_{E_i} - x_{F_i} m_{F_i} - x_{G_i} m_{G_i} - x_{H_i} m_{H_i} - x_{I_i} m_{I_i}}{m_i} \tag{53}$$

$$y_{S_i} = \frac{y_{A_i} m_{A_i} - y_{B_i} m_{B_i} - y_{C_i} m_{C_i} + y_{D_i} m_{D_i} + y_{E_i} m_{E_i} - y_{F_i} m_{F_i} - y_{G_i} m_{G_i} - y_{H_i} m_{H_i} - y_{I_i} m_{I_i}}{m_i} \tag{54}$$

The center of mass coordinates of the simplified portions are formulated in equations (55-63).

$$x_{A_i} = \frac{l_i + b_i + d_i}{2} - b_i \,,\; y_{A_i} = 0 \tag{55}$$

$$x_{B_i} = l_i \,,\; y_{B_i} = 0 \tag{56}$$

$$x_{C_i} = 0 \,,\; y_{C_i} = 0 \tag{57}$$

$$x_{D_i} = \frac{l_i + b_i + d_i}{2} - b_i \,,\; y_{D_i} = \frac{c_i + f_i}{2} \tag{58}$$

$$x_{E_i} = \frac{l_i + b_i + d_i}{2} - b_i \,,\; y_{E_i} = -\frac{c_i + g_i}{2} \tag{59}$$

$$x_{F_i} = \frac{1}{3} h_i - b_i,\; y_{F_i} = \frac{c_i}{2} + \frac{2}{3} f_i \tag{60}$$

$$x_{G_i} = l_i + d_i - \frac{1}{3} i_i \,,\; y_{G_i} = \frac{c_i}{2} + \frac{2}{3} f_i \tag{61}$$

$$x_{H_i} = \frac{1}{3} j_i - b_i,\; y_{H_i} = -\frac{c_i}{2} - \frac{2}{3} g_i \tag{62}$$

$$x_{I_i} = l_i + d_i - \frac{1}{3} k_i \,,\; y_{I_i} = -\frac{c_i}{2} - \frac{2}{3} g_i \tag{63}$$

The center of mass coordinates of the shafts are as follows:

$$x_{shaftB_2} = l_2 \,,\; y_{shaftB_2} = 0 \tag{64}$$

$$x_{shaftB_4} = l_4 \,,\; y_{shaftB_4} = 0 \tag{65}$$

3.2.2.3 Inertia.

The mass moment of inertia of a body is a property that measures the body's resistance to angular acceleration [27]. The moment of inertia value is different depending on the axis about which it is computed. However, the axis generally chosen for analysis passes through the body's center of mass. Therefore, the parallel axis theorem is used [27]. The inertias of the links are shown in equations (66-68).

$$I_2 = I_{S_2} + I_{shaftB_2} + I_{csC_2} \tag{66}$$

$$I_3 = I_{S_3} \tag{67}$$

$$I_4 = I_{S_4} + I_{shaftB_4} + I_{csC_4} \tag{68}$$

The sum of the inertias of the simplified portions of a link is as follows:

$$I_{S_i} = I_{A_i} - I_{B_i} - I_{C_i} + I_{D_i} + I_{E_i} - I_{F_i} - I_{G_i} - I_{H_i} - I_{I_i} \tag{69}$$

Equation (70) represents the change induced by the parallel axis.

$$P_{\#} = m_{\#}(\sqrt{(x_{\#} - x_{CM_i})^2 + (y_{\#} - y_{CM_i})^2})^2 \tag{70}$$

where the # represents the portion of the link or shaft being considered.

The inertias of the simplified portions are formulated in equations (71-79).

$$I_{A_i} = \frac{1}{12} m_{A_i}((l_i + b_i + d_i)^2 + {c_i}^2) + P_{A_i} \tag{71}$$

$$I_{B_i} = \frac{1}{2} m_{B_i}({r_B}^2) + P_{B_i} \tag{72}$$

$$I_{C_i} = \frac{1}{2} m_{C_i}({r_i}^2) + P_{C_i} \tag{73}$$

$$I_{D_i} = \frac{1}{12} m_{D_i}\left((l_i + b_i + d_i)^2 + {f_i}^2\right) + P_{D_i} \tag{74}$$

$$I_{E_i} = \frac{1}{12} m_{E_i}((l_i + b_i + d_i)^2 + {g_i}^2) + P_{E_i} \quad (75)$$

$$I_{F_i} = \frac{1}{18} m_{F_i}({f_i}^2 + {h_i}^2) + P_{F_i} \quad (76)$$

$$I_{G_i} = \frac{1}{18} m_{G_i}({f_i}^2 + {i_i}^2) + P_{G_i} \quad (77)$$

$$I_{H_i} = \frac{1}{18} m_{H_i}({g_i}^2 + {j_i}^2) + P_{H_i} \quad (78)$$

$$I_{I_i} = \frac{1}{18} m_{I_i}({g_i}^2 + {k_i}^2) + P_{I_i} \quad (79)$$

The inertias of the shafts and cylindrical supports are as follows:

$$I_{shaftB_2} = \frac{1}{2} m_{shaftB_2} \times {r_B}^2 + P_{shaftB_2} \quad (80)$$

$$I_{shaftB_4} = \frac{1}{2} m_{shaftB_4} \times {r_B}^2 + P_{shaftB_4} \quad (81)$$

$$I_{csC_{i_{2,4}}} = \frac{1}{2} m_{csC_{i_{2,4}}} \times ({r_{csC}}^2 + {r_i}^2) + P_{csC_{i_{2,4}}} \quad (82)$$

3.2.3 Coupled system modelling.

The dynamic model of the coupled four-bar mechanism is derived in detail in [7, 9]. The four-bar mechanism has one degree of freedom, which is the rotation of the crank. The actuator in this case is a DC motor. The schematic representation of the four-bar mechanism is shown in Figure 12.

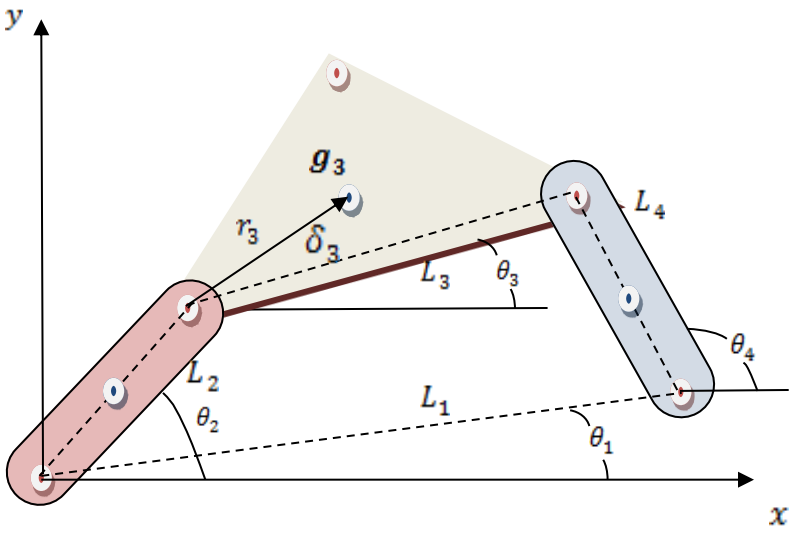

Figure 12: Four-Bar Mechanism

The kinematics of the mechanism is required for the dynamics analysis. The angular velocities of the links and the linear velocities of the centers of masses of the different moving links are given by equations (83-85).

$$\dot{\theta}_i = \gamma_i \dot{\theta}_2 \tag{83}$$

$$v_{ix} = \alpha_i \dot{\theta}_2 \tag{84}$$

$$v_{iy} = \beta_i \dot{\theta}_2 \tag{85}$$

where

$$\alpha_2 = -r_2 \sin(\theta_2 + \delta_2) \tag{86}$$

$$\alpha_3 = -L_2 \sin\theta_2 - r_3 \gamma_3 \sin(\theta_3 + \delta_3) \tag{87}$$

$$\alpha_4 = -r_4 \gamma_4 \sin(\theta_4 + \delta_4) \tag{88}$$

$$\beta_2 = r_2 \cos(\theta_2 + \delta_2) \tag{89}$$

$$\beta_3 = L_2 \cos\theta_2 - r_3 \gamma_3 \cos(\theta_3 + \delta_3) \tag{90}$$

$$\beta_4 = -r_4 \gamma_4 \cos(\theta_4 + \delta_4) \tag{91}$$

$$\gamma_2 = 1 \tag{92}$$

$$\gamma_3 = \frac{L_2 \sin(\theta_4 - \theta_2)}{L_3 \sin(\theta_3 - \theta_4)} \tag{93}$$

$$\gamma_4 = \frac{L_2 \sin(\theta_3 - \theta_2)}{L_3 \sin(\theta_3 - \theta_4)} \tag{94}$$

Defining the Lagrangian function,

$$L = K - V \tag{95}$$

where

$$K = \sum_{i=2}^{4} \left(\frac{1}{2} m_i \left(v_{ix}^2 + v_{iy}^2\right) + \frac{1}{2} J_i \dot{\theta}_i^2\right) = \frac{1}{2} A(\theta_2) \dot{\theta}_2^2 \tag{96}$$

$$A(\theta_2) = \sum_{i=2}^{4} \left(m_i (\alpha_i^2 + \beta_i^2) + \gamma_i^2 J_i\right) \tag{97}$$

The Euler-Lagrange formulation is given by equation (98).

$$T = \frac{d}{dt}\left(\frac{\partial L}{\partial \dot{\theta}_2}\right) - \frac{\partial L}{\partial \theta_2} \tag{98}$$

The partial and total derivatives of the Euler- Lagrange equation are equated to yield equation (99).

$$T_{mech} = A(\theta_2)\ddot{\theta}_2 + \frac{1}{2}\frac{dA(\theta_2)}{d\theta_2}\dot{\theta}_2^2 + \frac{dP}{d\theta_2} \tag{99}$$

where

$$A(\theta_2) = C_0 + C_1\gamma_3^2 + C_2\gamma_4^2 + C_3\gamma_3\cos(\theta_2 - \theta_3 - \delta_3) \tag{100}$$

$$\frac{dA(\theta_2)}{d\theta_2} = 2C_1\gamma_3\frac{d\gamma_3}{d\theta_2} + 2C_2\gamma_4\frac{d\gamma_4}{d\theta_2} + C_3\frac{d\gamma_3}{d\theta_2}\cos(\theta_2 - \theta_3 - \delta_3) - C_3\gamma_3(1 - \gamma_3)\sin(\theta_2 - \theta_3 - \delta_3) \tag{101}$$

$$C_0 = J_2 + m_2r_2^2 + m_3L_2^2 \tag{102}$$

$$C_1 = J_3 + m_3r_3^2 \tag{103}$$

$$C_2 = J_4 + m_4r_4^2 \tag{104}$$

$$C_3 = 2m_3L_2r_3 \tag{105}$$

$$\frac{d\gamma_3}{d\theta_2} = \frac{L_2(D_1 + D_2)}{L_3\sin^2(\theta_3 - \theta_4)} \tag{106}$$

$$\frac{d\gamma_4}{d\theta_2} = \frac{L_2(D_3 + D_4)}{L_4\sin^2(\theta_3 - \theta_4)} \tag{107}$$

$$D_1 = (\gamma_4 - 1)\sin(\theta_3 - \theta_4)\cos(\theta_4 - \theta_2) \tag{108}$$

$$D_2 = (\gamma_4 - \gamma_3)\sin(\theta_4 - \theta_2)\cos(\theta_3 - \theta_4) \tag{109}$$

$$D_3 = (\gamma_3 - 1)\sin(\theta_3 - \theta_4)\cos(\theta_3 - \theta_2) \tag{110}$$

$$D_4 = (\gamma_4 - \gamma_3)\sin(\theta_3 - \theta_2)\cos(\theta_3 - \theta_4) \tag{111}$$

$$\frac{dP}{d\theta_2} = g(m_2r_2\cos(\theta_2) + m_3(L_2\cos(\theta_2) + r_3\gamma_3\cos(\theta_3)) + m_4r_4\gamma_4\cos(\theta_4))\,\dot{\theta}_2 \tag{112}$$

In order to model the full dynamics of the four-bar mechanism, the dynamics of the actuator must be included. The DC motor schematic is shown in Figure 13.

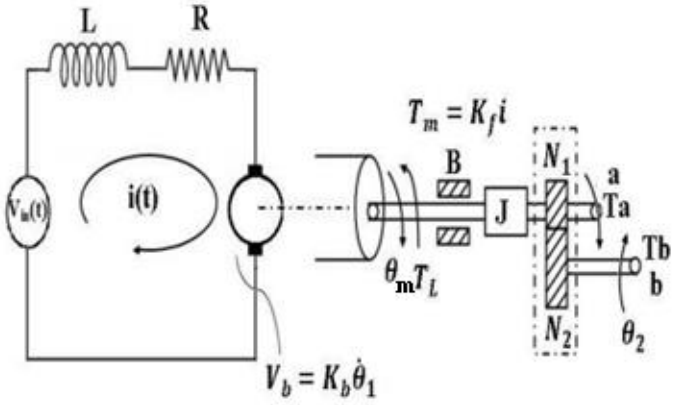

Figure 13: Schematic Diagram of a DC Motor

The electrical and mechanical equations of the DC motor are presented by equations (113-114):

$$L\frac{di(t)}{dt} + Ri(t) = V_{in}\,(t) - K_b\dot{\theta}_{\mathrm{m}} \tag{113}$$

$$T_m - B\dot{\theta}_{\mathrm{m}} - T_a - T_L\ = J\ddot{\theta}_{\mathrm{m}} \tag{114}$$

The mechanical transmission is given by the ratio in equation (115):

$$\frac{T_b}{T_a} = \frac{\dot{\theta}_{\mathrm{m}}}{\dot{\theta}_2} = \frac{r_2}{r_1} = \frac{N_2}{N_1} = n \tag{115}$$

Substituting *Ta* from (114) to (115) the output torque to the mechanical system is given by equation (116).

$$T_b = n(T_m - T_L\ - B\dot{\theta}_{\mathrm{m}} - J\ddot{\theta}_{\mathrm{m}}) \tag{116}$$

where J is the inertia of the motor and T_L is the constant load, due, for instance, to brush friction or gear friction.

Using the transmission angle relation in (115) and assuming that $T_L = 0$, equations (113, 116) can be formulated in terms of $\theta_2$as shown in (117, 118).

$$T_b = nK_f i(t)\ - n^2 B\dot{\theta}_2 - n^2\,J\ddot{\theta}_2 \tag{117}$$

$$L\frac{di(t)}{dt} + Ri(t) = V_{in}\,(t) - nK_b\dot{\theta}_2 \tag{118}$$

Hence, the coupled dynamics of the DC motor with the four-bar mechanism is given by combining the electrical and mechanical equations of the DC motor (117, 118) with mechanism dynamics (99) by equating the torque output from the motor to the torque required by the mechanism as in (119).

$$A(\theta_2)\ddot{\theta}_2 + \frac{1}{2}\frac{dA(\theta_2)}{d\theta_2}\dot{\theta}_2^2 + \frac{dP}{d\theta_2} = nK_f i(t)\ - n^2 B\dot{\theta}_2 - n^2\,J\ddot{\theta}_2 \tag{119}$$

The state variable vector is composed of the crank angle, the crank speed, and the motor current. The coupled dynamics in a state space representation of the DC motor with the four-bar mechanism is given by (121), where *x* is the state variable vector and *u(t)* is the input voltage.

$$\dot{x} = f(x, u(t), t) \tag{120}$$

$$\dot{x} = \begin{bmatrix} \dot{\theta}_2 \\ A_0[A_1\dot{\theta}_2^2 + A_2\dot{\theta}_2 + nK_f i - \frac{dP}{d\theta_2}] \\ \frac{1}{L}(V_{in}(t) - nK_b\dot{\theta}_2 - Ri) \end{bmatrix} \quad (121)$$

where

$$x = \begin{bmatrix} \theta_2 \\ \dot{\theta}_2 \\ i \end{bmatrix} \quad (122)$$

$$u(t) = V_{in}(t) \quad (123)$$

$$\mathrm{A_0} = \frac{1}{\mathrm{A}(\theta_2) + \mathrm{n}^2\,\mathrm{J}} \quad (124)$$

$$A_1 = -\frac{1}{2}\frac{dA(\theta_2)}{d\theta_2} \quad (125)$$

$$A_2 = -n^2 B \quad (126)$$

3.2.4 Dynamics validation.

Before moving to the optimization problem, the mechanism dynamics and the coupled system dynamics have to be validated. The mechanism and motor parameters used for validation are taken from [7] and are shown in Table 5 and Table 6.

Table 5: Validation Mechanism Parameters [7]

Mechanism parameters					
Link Length (m)		Center of mass location		Rectangular links	
L_1	0.56	r (m)	angle	depth (m)	height (m)
L_2	0.1	r_2 = 0.05	δ_2= 0	0.01	0.04
L_3	0.61	r_3 = 0.3	δ_3 = 0		
L_4	0.41	r_4 = 0.2	δ_4 = 0		

Table 6: Validation Motor Parameters [7]

Motor parameters					
R (Ω)	L (H)	km(Nm/A)	kg (Vs)	J (kg m^2)	B (Nms)
0.4	0.05	0.678	0.678	0.056	0.226

3.2.4.1 Mechanism dynamics.

Using the Lagrange formulation the mechanism dynamics are been derived in Section 3.2.3 . The mechanism torque, without adding a spring or a damper to the system, is shown in (127).

$$T_{mech} = A(\theta_2)\ddot{\theta}_2 + \frac{1}{2}\frac{dA(\theta_2)}{d\theta_2}\dot{\theta}_2^2 + \frac{dP}{d\theta_2} \tag{127}$$

The mechanism is simulated in cross configuration, as in Figure 14, running at a constant crank speed of 30 rad/s. The crank input torque obtained from the Lagrange formulation is compared with the results obtained from the Lagrange multipliers formulation [28] and Sim-mechanics shown in Figure 15.

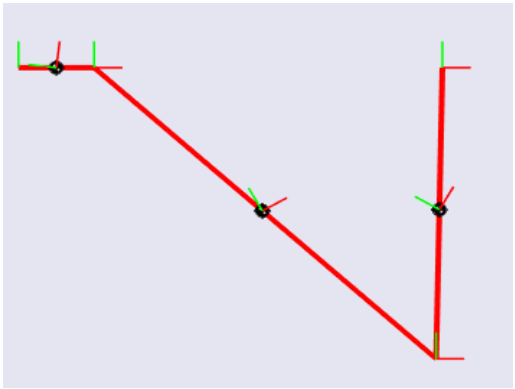

Figure 14: Mechanism Cross Configuration

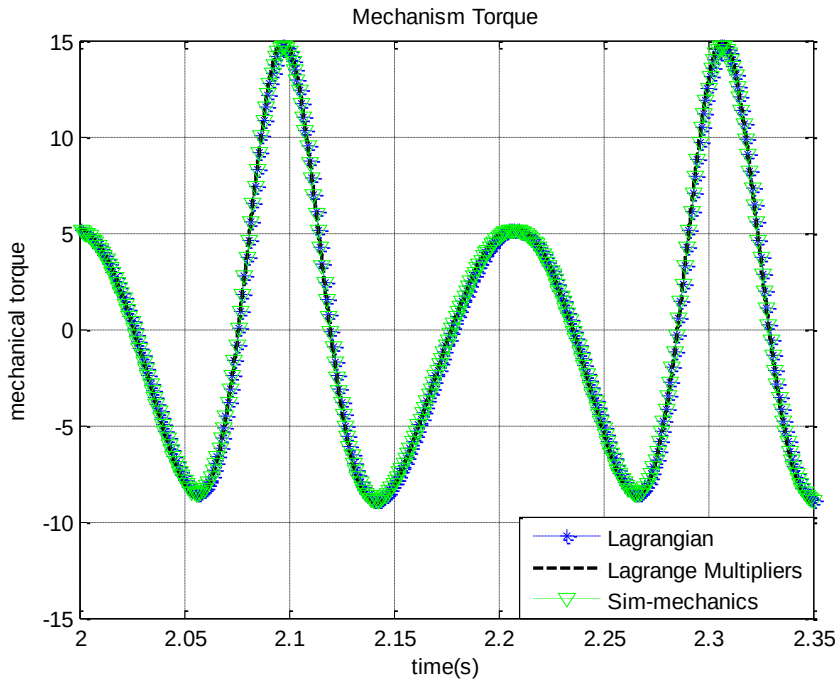

Figure 15: Mechanism Dynamics Validation

3.2.4.2 Coupled dynamics.

After validating the mechanism dynamics, the coupled dynamics of the mechanism-motor system need to be validated. The state space representation of the system was derived in Section 3.2.3 . Having the states as the crank angular position, speed, and current, this system of three first-order equations has been solved using the Runge-Kutta fourth-order method.

$$\dot{x} = f(x, u(t), t) \tag{128}$$

The mechanism is simulated in an open configuration, as in Figure 16, running the system at an input voltage of 30 V. The crank input torque and angular speed obtained from solving the ODEs is compared with the results obtained from Simscape at steady state, shown in Figure 17.

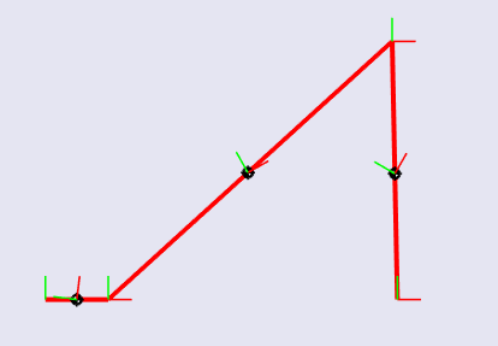

Figure 16: Mechanism Open Configuration

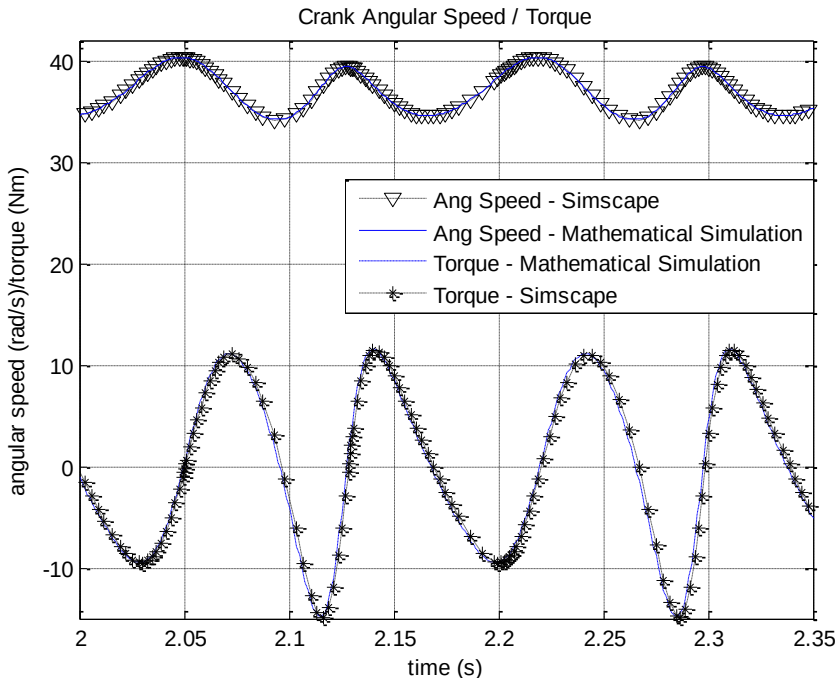

Figure 17: Coupled Dynamics Validation

3.2.5 Motors.

Selecting the best actuator to run a system is part of the design of any mechatronic system. A total of 13 motors are considered in the design problem out of which the most suited motor is selected to drive the system. The motors are selected based on their average and maximum torque characteristics as well as their maximum speed. This provides the optimization motors with a torque range to derive different loads obtained from different designs. The motors are considered to be part of the dynamics optimization problem as well as the motors' capability of driving the load. The motors in Table 7 are brushed DC motors from Pittman [29].

Table 7: Characteristics of the Candidate DC Motors

Motor	R (Ω)	L (H)	k_f (Nm/A)	k_b (Vs)	J (kg m^2)	B (Nms)	N (rev/min)	Average torque (Nm)	Max torque (Nm)
M1	4.02	2.44e-3	0.024	0.024	1.62e-6	1.01e-6	8980	0.0226	0.1426
M2	15.8	9.77e-3	0.049	0.049	1.62e-6	1.01e-6	8980	0.0226	0.1447
M3	4.33	2.34e-3	0.022	0.022	1.62e-6	1.34e-6	9960	0.0184	0.1172
M4	17	9.35e-3	0.044	0.044	1.62e-6	1.34e-6	9970	0.0184	0.1193
M5	2.74	2.57e-3	0.037	0.037	5.79e-6	3.36e-6	6003	0.0586	0.3198
M6	8.98	10.5e-3	0.075	0.075	5.79e-6	3.36e-6	5981	0.0586	0.3947
M7	1.85	1.97e-3	0.042	0.042	8.47e-6	3.69e-6	5230	0.0812	0.5422
M8	11.1	12.3e-3	0.106	0.106	8.47e-6	3.69e-6	5280	0.0812	0.5712
M9	1.01	1.6e-3	0.061	0.061	2.61e-5	1.21e-5	3630	0.1836	1.4402
M10	6.33	10.3e-3	0.156	0.156	2.61e-5	1.21e-5	3610	0.1836	1.4755
M11	0.24	0.31e-3	0.042	0.042	4.73e-5	1.68e-5	3330	0.353	2.6616
M12	0.93	1.4e-3	0.09	0.09	4.73e-5	1.68e-5	3140	0.353	2.9017
M13	3.64	5.58e-3	0.179	0.179	4.73e-5	1.68e-5	3150	0.353	2.9511

3.2.5.1 Motor-task feasibility.

Clearly, the maximum power of the motor has to be more than the peak power required by the task. However, this is not enough to decide the motor's capability of performing the task, as power consists of speed and torque, which are both limited in actuators. Hence, the feasibility analysis has to check for both components [30].

A motor-task combination is feasible if a transmission ratio (n) exists such that the motor's maximum speed is greater than the maximum required speed, and a certain norm of the motor torque is less than a corresponding motor-specific limit. The second norm of the torque is a measure of the "RMS" (Root Mean Square) current in the windings, which should be limited to avoid thermal destruction of the windings. The infinity norm is the measure of the peak current, which should be

limited to avoid demagnetization of the permanent magnets. The limit of the second norm is the rated motor torque and the limit of the infinity norm is the maximum motor torque [30].

Hence, for a motor to be able to drive the mechanism, the three inequalities (129-131) must hold. The maximum required crank speed has to be smaller than the motor's maximum speed, the RMS value of the required input torque should be smaller than the motor's rated torque, and the required peak torque should be smaller than the motor's peak torque [7, 31].

$$n\dot{\theta}_2 \leq N_{motor} \tag{129}$$

$$T_{mech,RMS} \leq n\, T_{motor,rated} \tag{130}$$

$$T_{mech,peak} \leq n\, T_{motor,peak} \tag{131}$$

3.2.6 Objective functions.

The use of optimization techniques to select the best motor and gear ratio for an application saves time and takes care of the motors' feasibility in running the load. If the voltage is set as the cost function, the optimization will also minimize the voltage required to run the load. For variable loads, like the four-bar mechanism, the voltage required to run the load at a certain speed is variable. In the case of the four-bar mechanism, the torque required fluctuates periodically in steady state due to the change of inertia over the cycle. This fluctuation can be seen as a fluctuation in the crank speed response as the motor is supplying the same voltage for a time-varying load. To run the mechanism at a constant speed, the motor has to provide a varying voltage to balance the effect of the varying load.

The design of the mechanical system's sizing and inertia parameters and motor and gear box selection are the goals of this problem. The objective functions are formulated here as to minimize the required voltage and voltage variation to run the mechanism at a constant speed.

The objective functions to be optimized are given by (132-133).

$$\mathrm{f}_1 : \min(\mathrm{V}) \tag{132}$$

$$\mathrm{f}_2 : \min\left(\frac{\mathrm{V}_{\max} - \mathrm{V}_{\min}}{\mathrm{V}_{\mathrm{avg}}}\right) \tag{133}$$

3.2.6.1 Design vector.

The design vector for the genetic algorithm is given by equation (134).

$$X = [\, b_{\mathrm{i}},\ c_{\mathrm{i}}, d_{\mathrm{i}},\ e_i,\ f_i, g_i, h_{\mathrm{i}},\ i_{\mathrm{i}}, j_{\mathrm{i}}, k_i,\ M_{\#}, \mathrm{n}\,] \tag{134}$$

The design vector is made of 32 variables. The index i represents the link number and the variables $b, c, d, e, f, g, h, i, j, k$ represent 10 variables for the dimensions of each link. The motor number and gear ratio are represented by $M_{\#}$, and n, respectively.

3.2.6.2 Constraints.

The optimization is subject to some motor feasibility constraints that are to be satisfied by the fittest individuals. The three constraints for the dynamics problem are the average torque, maximum torque, and maximum speed required from the motor. These constraints are shown in inequalities (129-131).

Each design variable is bound in a range as shown in (135).

$$g_1(x)\colon x_i \in [\, x_{i\,min},\ x_{i\,max}] \tag{135}$$

Using the penalty method, the objective function can be written as:

$$\mathrm{f_1}\colon \min(\mathrm{V} + \mathrm{m_1} \times \mathrm{C_1} + \mathrm{m_2} \times \mathrm{C_2} + \mathrm{m_3} \times \mathrm{C_3}) \tag{136}$$

$$\mathrm{f_2}\colon \min\left(\frac{\mathrm{V_{max}} - \mathrm{V_{min}}}{\mathrm{V_{avg}}}\right) \tag{137}$$

where C_1, C_2, and C_3 are constants corresponding to the speed and torque constraints (0 if the constraint is satisfied and 1 otherwise). m_i is a high value real number that penalizes the objective function if the constraint is not met. The value for m_i should be greater than the value of the minimized objective.

3.2.7 Example problem.

The objective is to find the mechanism inertia and select the adequate motor and gear ratio that will minimize the required voltage and voltage variation to run the mechanism at a constant speed of 30 rad/s. The mechanism's link lengths are shown in Table 8.

Table 8: Mechanism Link Parameters

Mechanism parameters			
$\mathrm{L_1(m)}$	$\mathrm{L_2(m)}$	$\mathrm{L_3(m)}$	$\mathrm{L_4(m)}$
0.56	0.1	0.61	0.41

3.2.7.1 Genetic algorithm.

To start with, three constraints are set that are to be satisfied by the fittest individuals. Bounded ranges are specified for the design variables. These bounds are shown below.

$$0.015 < b_i, d_i < 0.3$$

$$0.03 < c_i < 0.1$$

$$0.006 < e_i < 0.03$$

$$0 < f_i, g_i < 0.1$$

$$0 < h_i, i_i, j_i, k_i < 0.1$$

$$1 < M_{\#} < 13$$

$$1 < n < 45$$

The fitness scaling function is the function used to convert the raw fitness scores to values suitable for the selection process. A good fitness scaling function considers both fitness and diversity. The scaling function used is based on the rank of the individual in the population. An individual with rank r has a scaled score of $1/\sqrt{r}$ [20]. Rank scaling gives high expectations for highly ranked individuals and low expectations for poorly ranked individuals, yet poorly ranked individuals have a probability of being selected to the next generation and increasing the diversity of the population.

The selection function specifies the choice of parents for the next generation. The selection function adopted for the genetic multi-objective optimization in Matlab is the tournament selection function which creates sized tournaments between random individuals. The best in each tournament qualifies to be a parent for the next generation.

The Pareto fraction specifies the fraction of the population on the Pareto front and the remaining fraction is used in searching the design space.

The selected options for the MOGA are shown in Table 9.

Table 9: Dynamics GA Options

Option	Choice
Population size	10000
Generations	450
Pareto fraction	0.76
Crossover fraction	0.5
Scaling function	Rank
Selection function	Tournament
Mutation function	Adaptive feasible
Crossover function	Heuristic

Running the MOGA, the obtained Pareto front is shown in Figure 18.

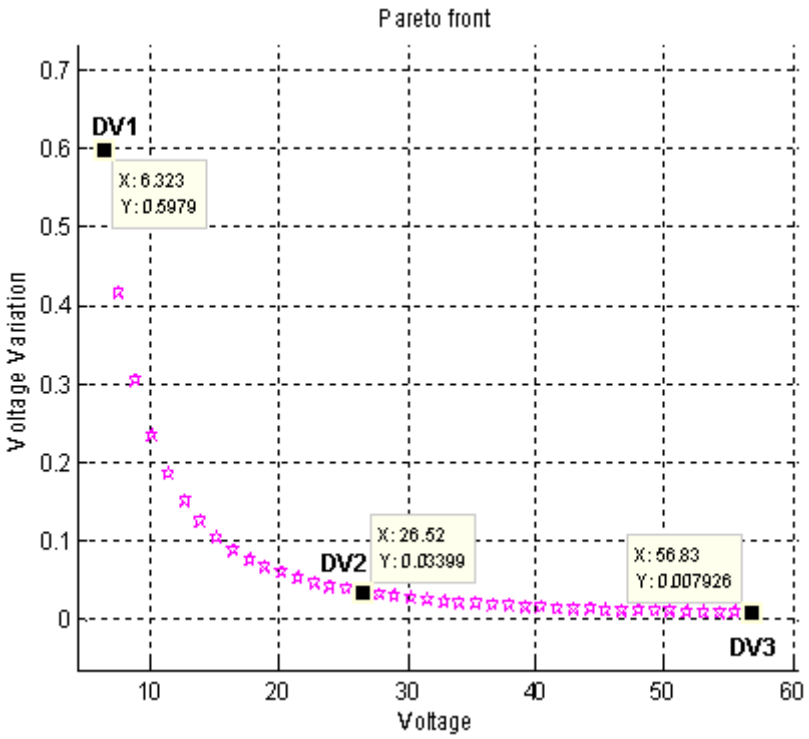

Figure 18: Dynamics Pareto Front

3.2.7.2 Results.

The Pareto front in Figure 18 provides a set of solutions to be chosen from. The tradeoff between voltage and voltage fluctuation can be observed and the designer can choose what best suites the application. Out of these solutions three designs labeled DV1, DV2, and DV3 are computed and the resulting design vectors are shown in Table 10 and Table 11.

Table 10: Geometric Parameters of the Selected Mechanisms

Mechanism parameters											
DV	(m)	b_i	c_i	d_i	e_i	f_i	g_i	h_i	i_i	j_i	k_i
1	L_2	0.2049	0.0970	0.1191	0.0150	0.0461	0.0346	0.0580	0.0254	0.0732	0.0359
	L_3	0.3000	0.3000	0.0150	0.0060	0.0000	0.0000	0.0664	0.0557	0.0183	0.0798
	L_4	0.0166	0.0301	0.0150	0.0060	0.0000	0.0000	0.0690	0.0570	0.0263	0.0811
2	L_2	0.1818	0.0963	0.1656	0.0132	0.0207	0.0120	0.0723	0.0340	0.0892	0.0227
	L_3	0.3000	0.3000	0.0150	0.0060	0.0000	0.0000	0.0438	0.0566	0.0488	0.0529
	L_4	0.0254	0.0300	0.0150	0.0060	0.0000	0.0000	0.0856	0.0041	0.0065	0.0823
3	L_2	0.2106	0.0411	0.0588	0.0117	0.0445	0.0901	0.0363	0.0541	0.0387	0.0277
	L_3	0.3000	0.0302	0.0165	0.0061	0.0005	0.0000	0.0878	0.0996	0.0339	0.0606
	L_4	0.0566	0.0312	0.0183	0.0060	0.0012	0.0006	0.0068	0.0662	0.0453	0.0886

Table 11: Motors Parameters

Motor parameters								
DV	M#	R (Ω)	L (H)	km (Nm/A)	kg (Vs)	J (kg m^2)	B (Nms)	n
1	11	0.24	0.31e-3	0.042	0.042	4.73e-5	1.68e-5	5
2	11	0.24	0.31e-3	0.042	0.042	4.73e-5	1.68e-5	21
3	11	0.24	0.31e-3	0.042	0.042	4.73e-5	1.68e-5	45

The voltage fluctuation required to run the mechanism at a constant speed is computed and the mean voltage is given as constant input voltage to the mechanism to see the effect on the crank angular speed response (see Figure 19, Figure 20, and Figure 21). It can be noticed that the smaller the voltage fluctuation compensation to run at a constant speed, the smaller the speed response fluctuation to the input average voltage.

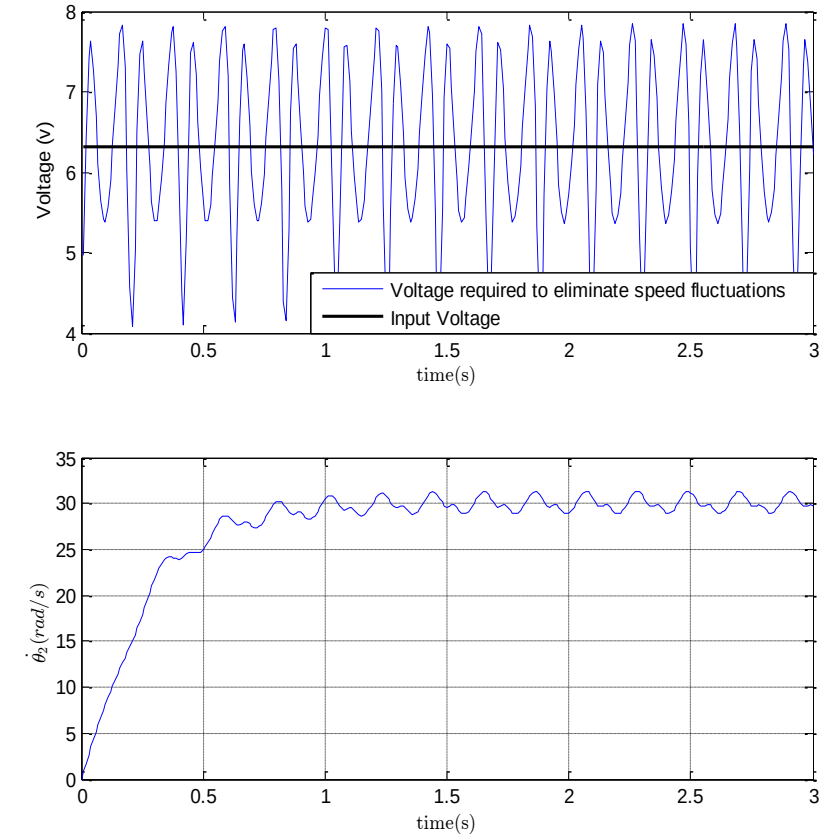

Figure 19: DV1 Input Voltage and Speed Response

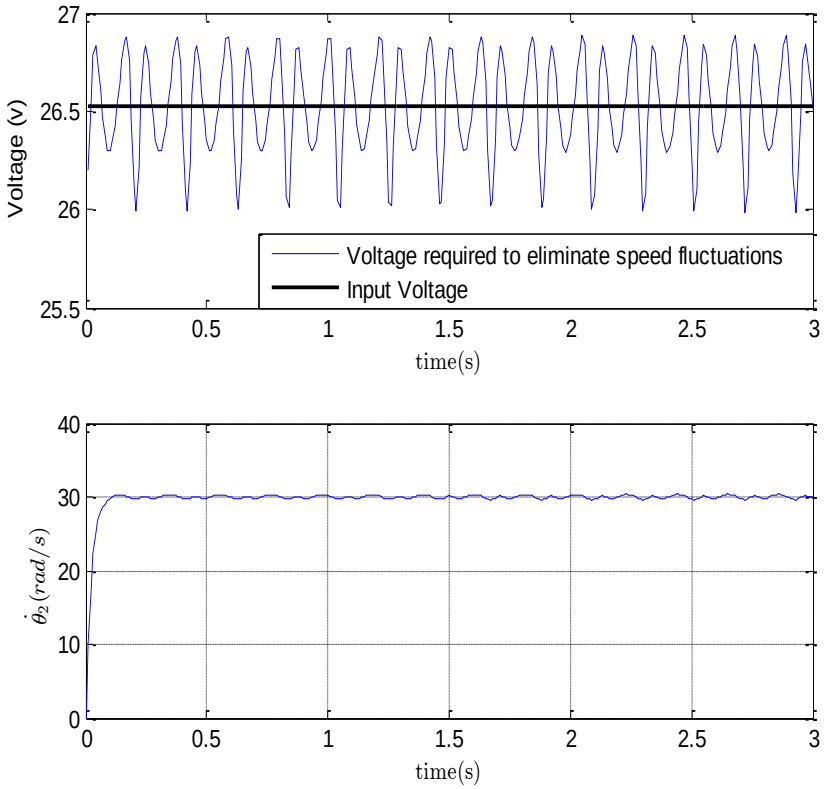

Figure 20: DV2 Input Voltage and Speed Response

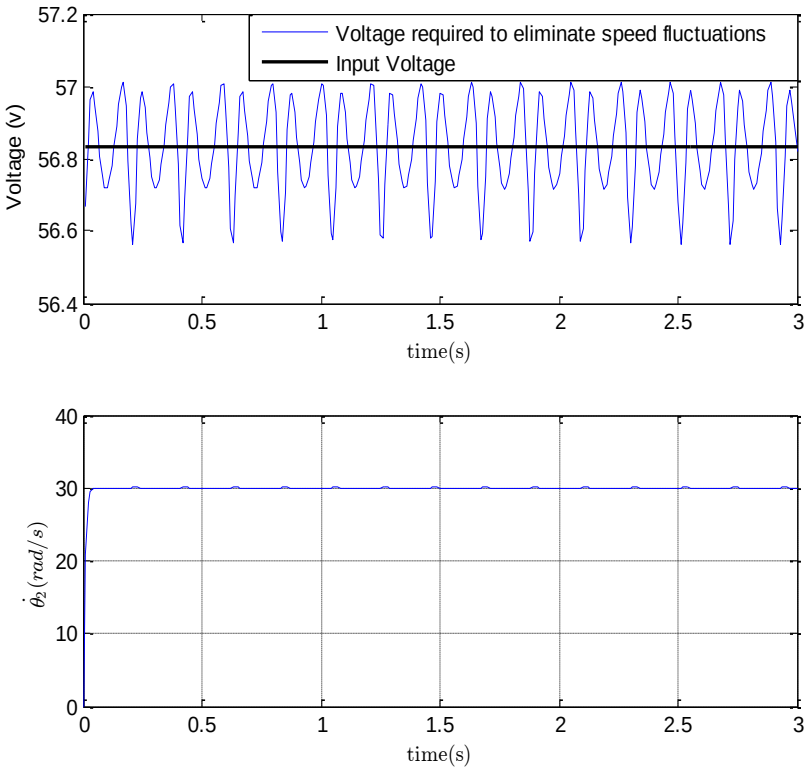

Figure 21: DV3 Input Voltage and Speed Response

3.3 Control

3.3.1 Introduction.

After considering the plant design, the system response is analyzed to check whether the response specifications and performance requirements can be met by the system. If the specifications cannot be met, a control system is designed to obtain the desired performance [32]. A control system is an interconnection of components forming a system configuration that will provide a desired system response [33].

The goal of control engineering design is to obtain the configuration, specifications, and identification of the key parameters of a proposed system to meet an actual need. The first step in the design process consists of establishing the system goals, for example stating the goal as to control the velocity of a motor accurately. The second step is to identify the variables that are desired to be controlled (for example, the velocity of the motor). The third step is to write the specifications in terms of the accuracy needed [33].

Once the system parameters are fixed, the system poles as well as its response are fixed. The control system alters the poles' locations to yield the desired response. In the early days, the design of controllers was mainly by trial and error. From this emerged an almost universal controller, the proportional-integral-derivative (PID) controller [34].

3.3.2 PID control.

The PID controller has been developed through much experience and by trial and error. Starting with the proportional feedback gain for amplifying a signal, integral control action was then discovered by engineers to eliminate bias offset. Finally, an "anticipatory" derivative term was added to enhance the poor dynamic response encountered in many cases [34]. The PID controller takes in the output of the system, which is the variable to be controlled (in this case the motor speed, subtracted from the reference or desired value). This difference or error is multiplied by a proportional gain, integrated and multiplied by an integral gain, derived and multiplied by a derivative gain. These three values are then added together and fed in as an input to the system. This loop continues and after some time the error goes to zero and the steady state value is equal to the desired value.

Tao and Sadler in [35] proposed a more robust modified PID controller represented by the control law in equation (138).

$$u(t) = K_p e(t) \int_0^t \dot{\theta}_2^d dt + K_i \int_0^t e(t)dt + K_d \dot{e}\,(t) \tag{138}$$

The difference between this controller and the conventional PID controller is the time varying integral in the proportional term of the controller. The resulting time varying proportional gain is also a function of the desired crank speed. As the desired speed or time increases, the gain increases, making the control system more robust [35].

Generally speaking, the higher the proportional gain the lower the speed fluctuation and the steady-state error. But, excessively high gains may lead to a large amount of overshoot if the derivative gain is not large enough. Increasing the derivative gain will decrease the overshoot, but the system response will be slower during the start-up period [35].

Formulating the design problem as an optimization problem will take care of the trade-off in design to meet system specifications and requirements.

The block diagram of the closed-loop system is shown in Figure 22.

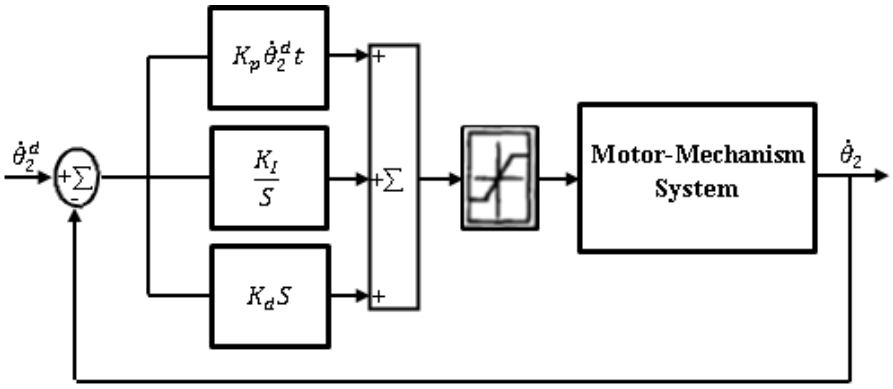

Figure 22: Closed-Loop System

3.3.3 System response.

The state space representation of the motor-mechanism system in (121) was derived in Section 3.2.3 . The states of the system are the crank angular position, speed, and current. Giving a voltage input to the motor and solving the state space equations using the Runge-Kutta fourth-order method, the time response of the crank angular position, speed, acceleration, the motor input current and its rate are obtained as well as the input torque.

Setting the input voltage to the system to be equivalent to the control law (138) discussed in Section 3.3.2, the closed-loop response of the system is obtained.

3.3.4 Objective function.

The use of optimization techniques to design a controller takes care of the design trade-off in the system response and will find the gain terms suitable to run the system at the desired specifications. The design of a constant motor speed controller is the goal of this problem. The optimization problem can be formulated in different ways. The objective function is formulated here as to minimize the derivative gain given that the system meets the overshoot, rise time, and steady state error requirements.

The objective function to be optimized is given by (139).

$$f_1: \min(K_d + m_1 \times C_1 + m_2 \times C_2 + m_3 \times C_3) \quad (139)$$

where $C_1, C_2,$ and C_3 are constraints on the system specifications to be met by the optimization problem and m_i is a high-value number that penalizes the objective function if the constraint is not met.

3.3.4.1 Design vector.

The design vector for the genetic algorithm is given by (140).

$$X = [K_p, K_i, K_d\ ] \tag{140}$$

The design vector is made of 3 variables: the proportional, integral, and derivative gains, respectively.

3.3.4.2 Constraints.

The optimization is subject to some system requirement constraints that are to be satisfied by the fittest individuals. The three constraints for the control problem are the overshoot, rise time, and steady state error requirements as discussed below.

The first constraint is the rise time specification which is less than 0.1 s for the motor speed response.

$$C_1: t_r\ \leq\ 0.1\ s$$

The second constraint is the response overshoot requirement of less than 1.7 % [35].

$$C_2: \dot{\theta}_2(t_r) \leq \dot{\theta}_2^d + 0.017\dot{\theta}_2^d$$

The steady state error is the third constraint and is less than 1 %.

$$C_3: S.S.E. \leq\ 0.01$$

Each design variable is bound in a range as shown in (141).

$$g_1(x): x_i \in [\ x_{i\ min},\ x_{i\ max}] \tag{141}$$

3.3.5 Case study.

The objective is to find the minimal gains required to meet the system requirements and specifications. This case study compares the objective function used here and in [31] and formulates the control optimization problem to be later used in the design problem. The mechanism and motor parameters used in this problem are shown in Table 12 and Table 13.

Table 12: Mechanism Parameters [35]

Mechanism parameters					
Link Length (m)		Center of mass location		Mass and inertia	
L_1	0.5593	r (m)	angle	mass (kg)	J (kg m^2)
L_2	0.102	r_2 = 0	δ_2= 0	1.362	0.00071
L_3	0.61	r_3 = 0.305	δ_3 = 0	1.362	0.0173
L_4	0.406	r_4 = 0.203	δ_4 = 0	0.2041	0.00509

Table 13: Motor Parameters [35]

Motor parameters					
R (Ω)	L (H)	km (Nm/A)	kg (Vs)	J (kg m^2)	B (Nms)
0.4	0.05	0.678	0.678	0.056	0.226

The crank angular speed open-loop response is shown in Figure 23.

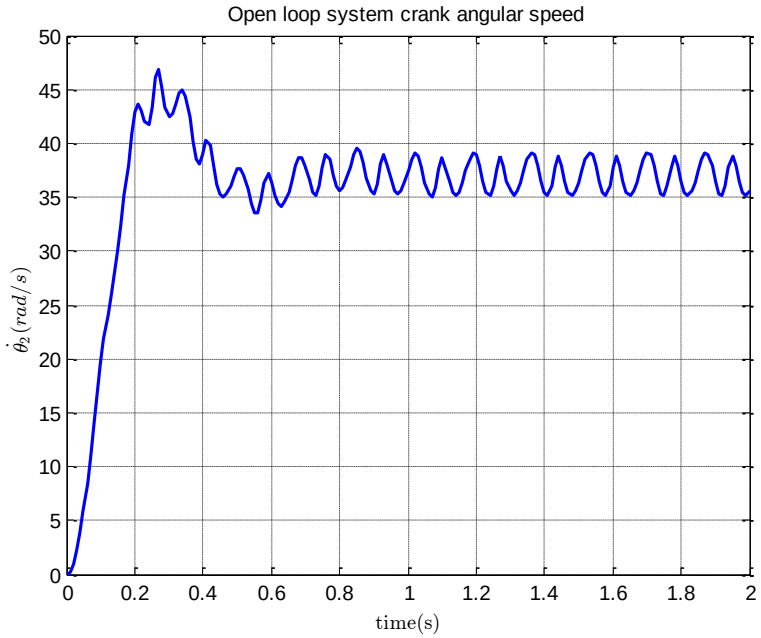

Figure 23: Crank Speed Open-Loop Response

3.3.5.1 Genetic algorithm.

To start, three constraints are set to be satisfied by the fittest individuals. Bounded ranges are specified for the design variables; these bounds are shown below.

$$0 < K_p, K_i, K_d < 100$$

The fittest individuals are to meet the system specifications.

The fitness scaling function is the function used to convert the raw fitness scores to values suitable for the selection process. A good fitness scaling function considers both fitness and diversity. The scaling function used is based on the rank of the individual in the population. An individual with rank r has a scaled score of $1/\sqrt{r}$ [20]. Rank scaling gives high expectations for highly ranked individuals and low expectations for poorly ranked individuals, yet poor individuals have a probability of being selected to the next generation and increasing the diversity of the population.

The selection function specifies the choice of parents for the next generation. The selection function can be stochastic uniform in which the scaled scores of the individuals in the current population make up a line with each individual having a proportional section of the line. The algorithm allocates a parent from the section it lands on randomly. The remainder function chooses parts based on the integer part of the individual scaled values [20]. There is also roulette selection, in which the parents are selected by simulating a roulette wheel. The individuals' expectation is translated into an area on the roulette wheel. The tournament selection function creates sized tournaments between random individuals and the best in each tournament qualifies to be a parent for the next generation.

A Monte Carlo study is done to check which of these selection functions is more suitable to the problem. The results for GA with different selection functions computed over 5 iterations are shown in Figure 24, where functions 1, 2, 3, and 4 are the stochastic uniform, remainder, roulette, and tournament, respectively.

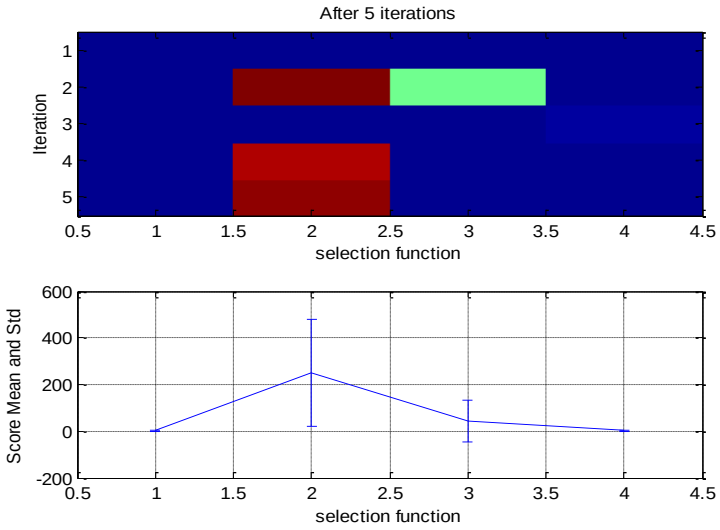

Figure 24: Choosing GA Selection Function - Control

In Figure 24, the top portion represents a color map of the minimized objective function values over the 5 iterations and the darker the color the smaller the value. The lower portion shows the mean and standard deviations of the values obtained over the 5 iterations. It can be noticed that the stochastic uniform and the tournament functions yield the lowest mean and standard deviation and hence are more suitable to be used as a selection function than the other methods.

After selecting the parents for the next generation, we select the portion of the offspring due to crossover and the portion due to mutation and the used functions. The mutation function used is adaptive feasible; this function randomly generates directions adaptive with the last generation and with a step size that satisfies the bounds. The crossover function choice is going to be from the intermediate, heuristic, and arithmetic crossover functions.

A Monte Carlo study was done to select the crossover function suitable for this problem shown in Figure 25, where functions 1, 2, and 3 are the intermediate, heuristic, and arithmetic, respectively.

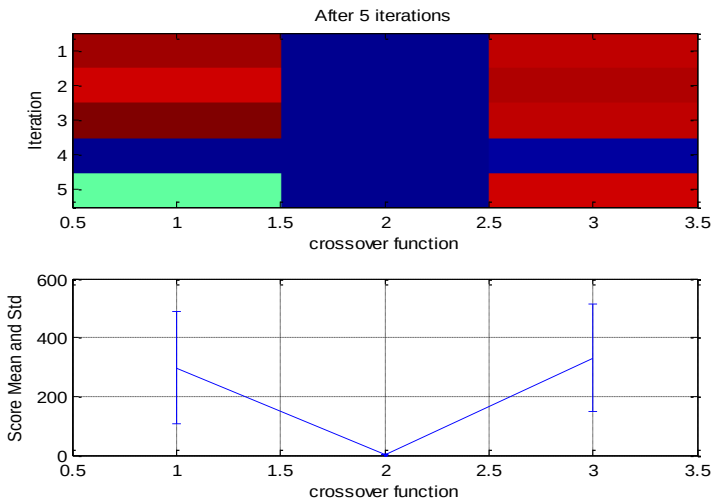

Figure 25: Choosing GA Crossover Function - Control

A GA is simulated for 5 iterations using each of the crossover functions and from the obtained objective function values the heuristic crossover function yielded the lowest mean and standard deviation. Now that the heuristic crossover function is selected, the heuristic crossover ratio and the crossover fraction of the generated offspring are chosen in the same manner.

By running some Monte Carlo studies, the options used to run the GA are selected and shown in Table 14.

Table 14: Control GA Options

Option	Choice
Population size	100
Generations	200
Elite count	4
Crossover fraction	0.76
Scaling function	Rank
Selection function	Stochastic uniform
Mutation function	Adaptive feasible
Crossover function	Heuristic

Running the GA, the best fit individual after 200 generations and the average of the generations are shown in Figure 26.

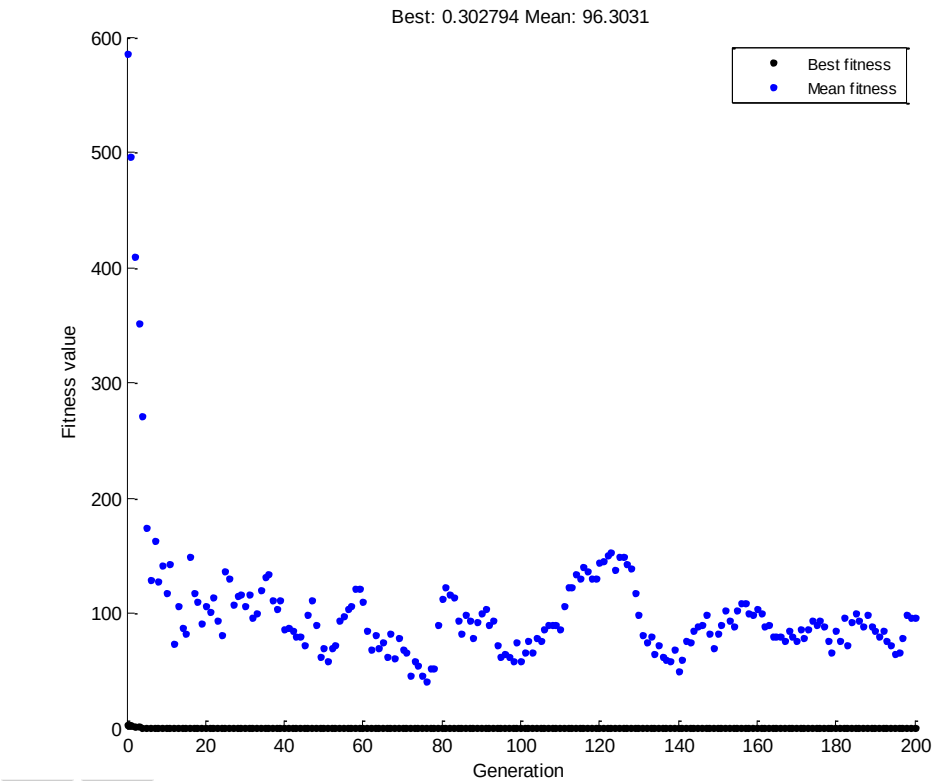

Figure 26: Control GA Analysis

3.3.5.2 Results.

The resulting design vector and the objective function value, which represents the derivative gain, are shown below:

$$\text{X: } [\ 11.7298, 0.1000, 0.3028]$$

$$\text{fval: } 0.3028$$

Computing the closed-loop response of the system, Figure 27 shows the crank angular speed response subject to the above control gains.

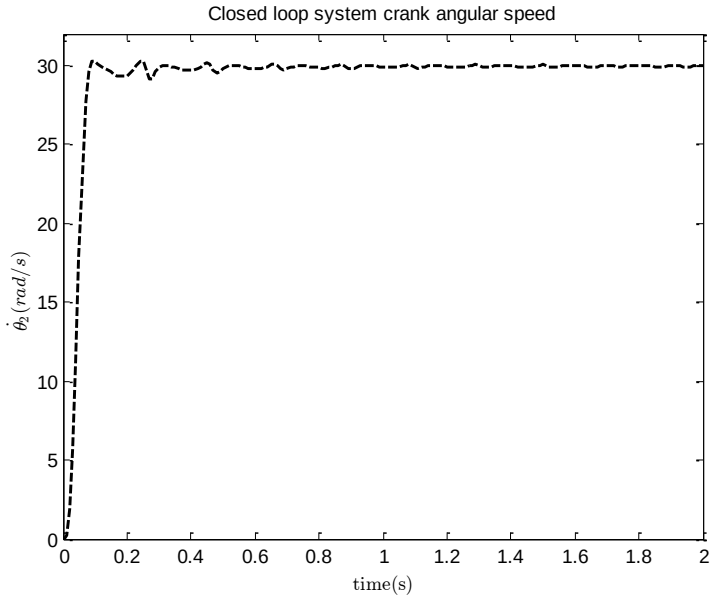

Figure 27: Crank Speed Closed-Loop Response with OS 1.3 %

The crank angular speed response has a rise time of 0.0448 s, an overshoot of 1.325 % and a steady state error of 1 %.

Tao and Sadler in [35] aimed to find the gains required to reduce the crank angular speed fluctuation. The response obtained by minimizing K_d and the one obtained by minimizing the speed fluctuation are shown in Figure 28 and a zoomed view in Figure 29. It can be seen that both solutions satisfy the specifications of 0.1 s rise time, an overshoot of 1.5 %, and a steady state error of 1 %. The response obtained by Tao and Sadler is better in terms of speed fluctuation as well as having the specifications of 0.0365 s rise time, an overshoot of 0.2 % and a steady state error of 0.25 %. They obtained the required control gains to be $[K_p = 43.25, K_i = 1.622, K_d = 0.739]$ compared to the gains obtained $[\ 11.7298, 0.1000, 0.3028]$ for a

rise time of 0.0448 s, an overshoot of 1.325 % and a steady state error of 1 %. This means that depending on the application, whether or not this difference in specifications is significant, our solution is considered better in terms of the control effort.

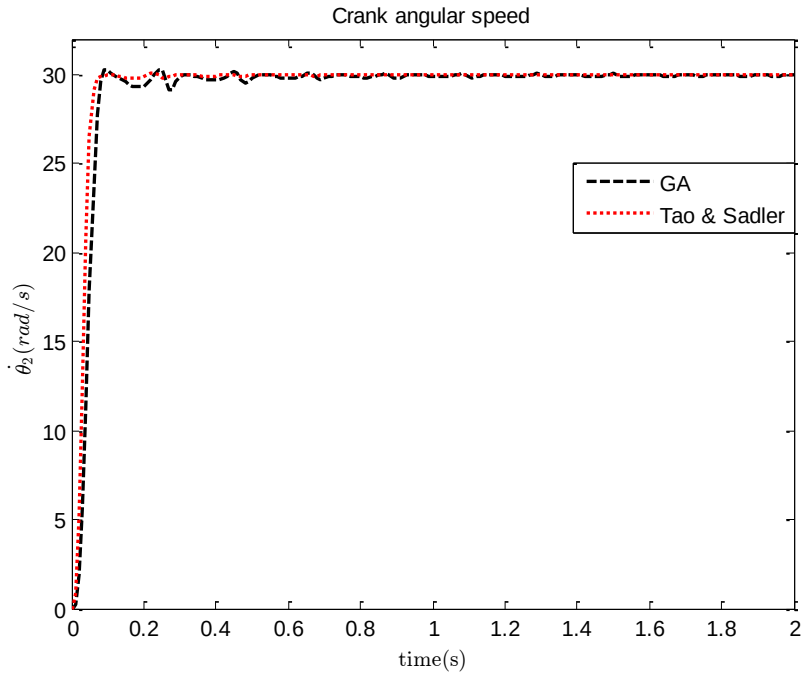

Figure 28: Crank Speed Closed-Loop Responses Comparison - OS 1.3 %

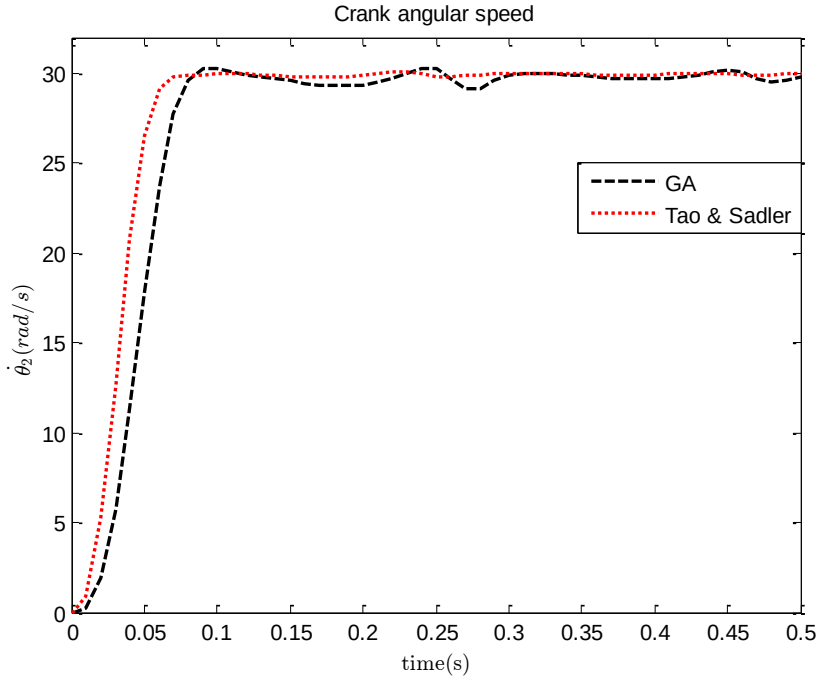

Figure 29: Crank Speed Closed-Loop Transient Responses Comparison - OS 1.3 %

To better compare the optimization problems, the constraints on the specifications are reduced to match the response obtained by Tao and Sadler. That is, the new constraints for the optimization problem are 0.0365 s rise time, an overshoot of 0.2 %, and a steady state error of 0.25 %. Running the optimization problem, the resulting design vector and the objective function value are shown below:

$$X: [\, 39.8556, 0.1000, 0.6392]$$

$$fval: 0.6392$$

Computing the closed-loop response of the system, Figure 30 shows the crank angular speed response subject to the above control gains. The crank angular speed response has a rise time of 0.0345 s, an overshoot of 0.2 %, and a steady state error of 0.25 %.

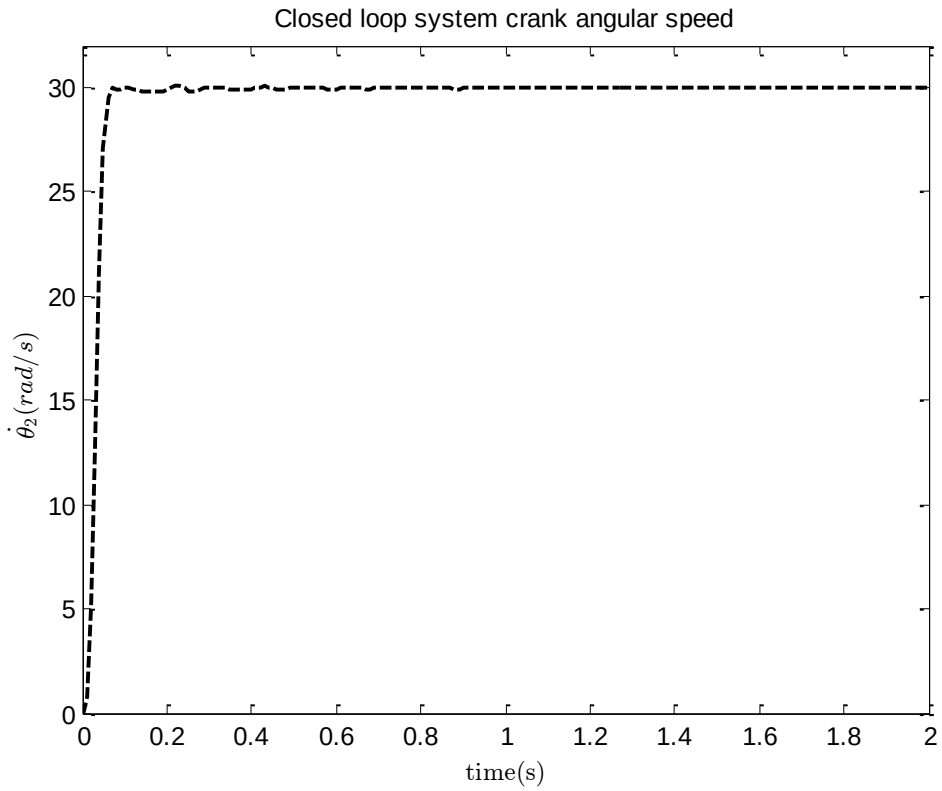

Figure 30: Crank Speed Closed-Loop Response with OS 0.2 %

The solution obtained is compared with the solution obtained by Tao and Sadler and the results are presented in Figure 31 and Figure 32.

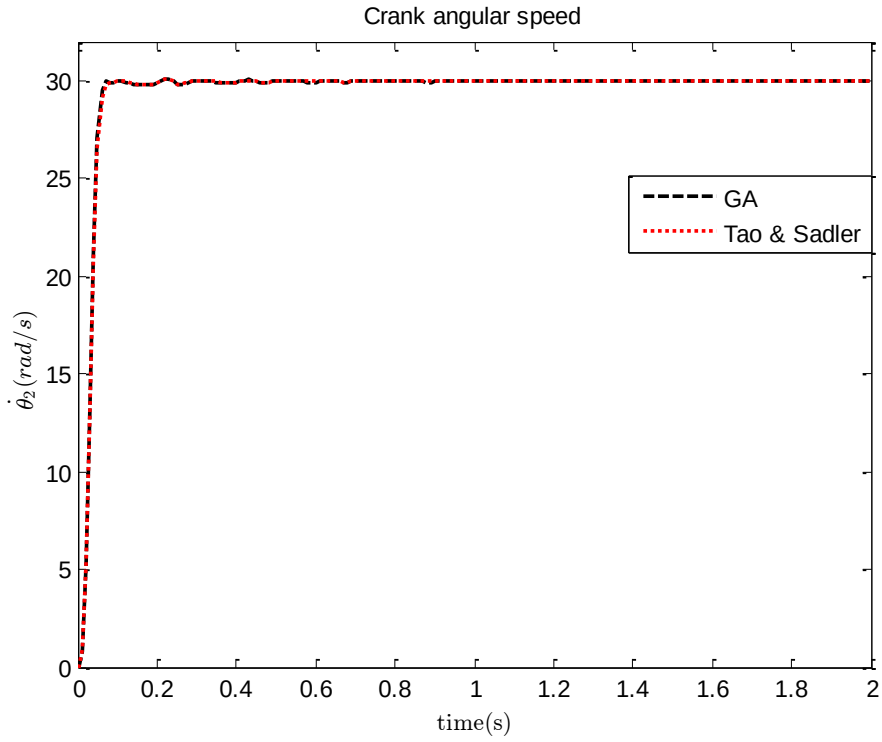

Figure 31: Crank Speed Closed-Loop Responses Comparison - OS 0.2 %

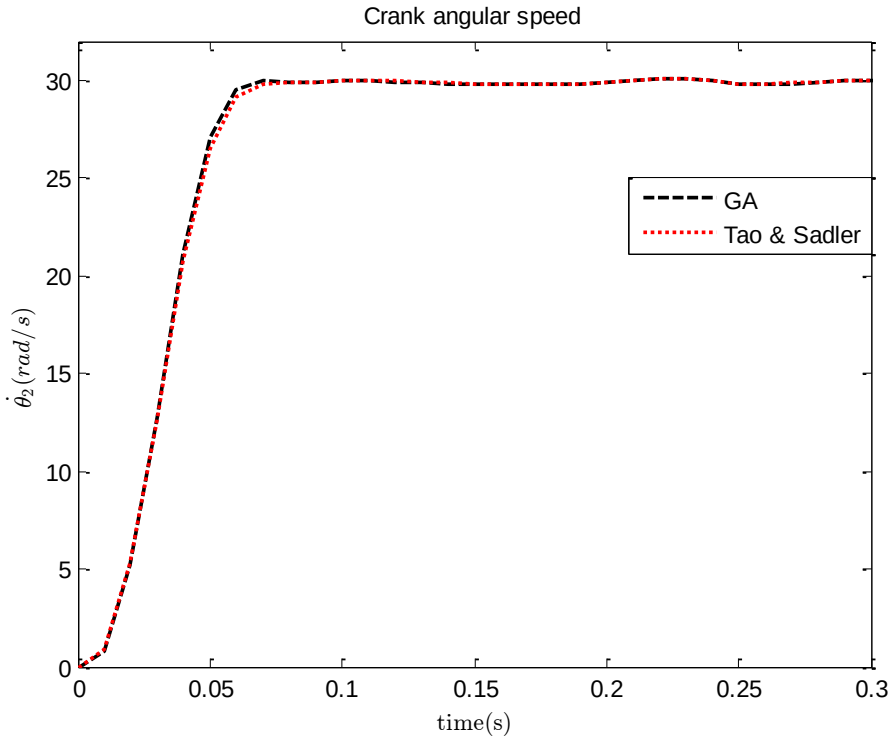

Figure 32: Crank Speed Closed-Loop Transient Responses Comparison - OS 0.2 %

The specifications and gains of both responses are shown in Table 15.

Table 15: Control Specifications and Gains

	Specifications			Gains		
	Rise time (s)	Overshoot (%)	S.S.E (%)	K_p	K_i	K_d
Solution	0.0345	0.200	0.25	39.8556	0.1000	0.6392
Tao & Sadler	0.0365	0.1977	0.25	43.25	1.622	0.739

It can be seen that by setting the desired specifications as constraints and minimizing the derivative gain, we meet the response requirements as well as minimize the gains.

Chapter 4: Optimization Results

4.1 Design Problem

The objective of this chapter is to compare the obtained design using the sequential approach to the one obtained by the holistic approach. The objective functions to be optimized are the desired path, the input voltage (required to run at 30 rad/s), and the control gains to meet a desired rise time, overshoot, and steady-state error. It is also desired to select the motor-gearbox combination required to run the system. Due to the high number of objectives, there is no one solution that will provide the best results for all these requirements due to the complex relations and multidisciplinary nature of the design; tradeoffs have to be made.

The conventional sequential design method will be considered first. In this case, the mechanical design is optimized and the obtained result is then optimized for its dynamics and its actuator. The control gains are then optimized for the obtained design. The holistic approach considers all the objective functions simultaneously and presents a set of non-dominated solutions as a Pareto front. The results from the two approaches will then be compared.

The desired path is shown in Figure 33.

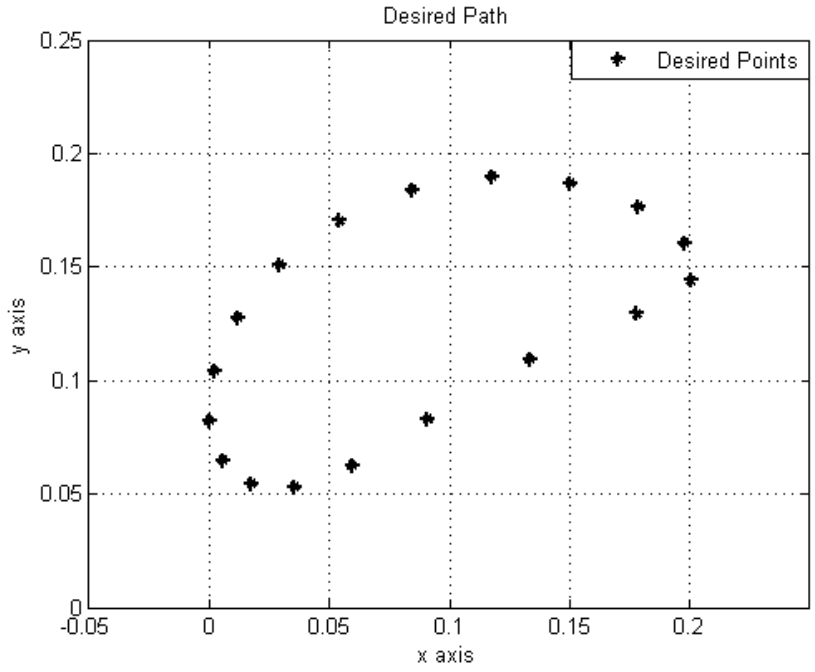

Figure 33: Design Desired Path

4.2 Sequential Approach

4.2.1 Synthesis.

It is desired to design a four-bar mechanism to trace a path of eighteen precision points using a genetic algorithm (Figure 33). The desired points are given below:

C_d^i = [(0.1778,0.1294) ; (0.2004,0.1441); (0.1976,0.1607) ; (0.1786,0.1765) ; (0.1503, 0.187) ; (0.1176,0.1898) ; (0.0844,0.1841) ; (0.0542,0.1705) ; (0.0294,0.1509) ; (0.0117,0.1279) ; (0.0019,0.1041) ; (0.0,0.0822) ; (0.0056,0.0649) ; (0.0177,0.0545) ;(0.0356,0.0531) ; (0.0593,0.0625) ; (0.0910,0.0829) ; (0.1335,0.1092)]

After optimizing the error, calculated as the square root of the sum of the square errors, the obtained design vector and error is given below:

X: [0.0432, 0.0000, 0.0173, 0.1900, 0.0851, 0.2465, 0.1806, 0.1241, 0.0616, 0.0004]

$$fval: 0.00119$$

Computing a hybrid function, the minimization function value reduces to:

$$fval: 0.000154$$

The resulting mechanism design (Table 16) is chosen and the design is fixed.

Table 16: Mechanism Links Design

Mechanism Design Vector (X)									
x_0(m)	y_0(m)	θ_1(rad)	L_1(m)	L_2(m)	L_3(m)	L_4(m)	r_{cx}(m)	r_{cy}(m)	$\theta_{2,0}$(rad)
0.0434	-0.0003	0.0022	0.1899	0.0849	0.2507	0.1884	0.1251	0.0602	0.0008

The design vectors obtained from the genetic algorithm and the hybrid minimization are computed and the resulting mechanisms are simulated. Next, the coupler paths are compared with the desired path as shown in Figure 34.

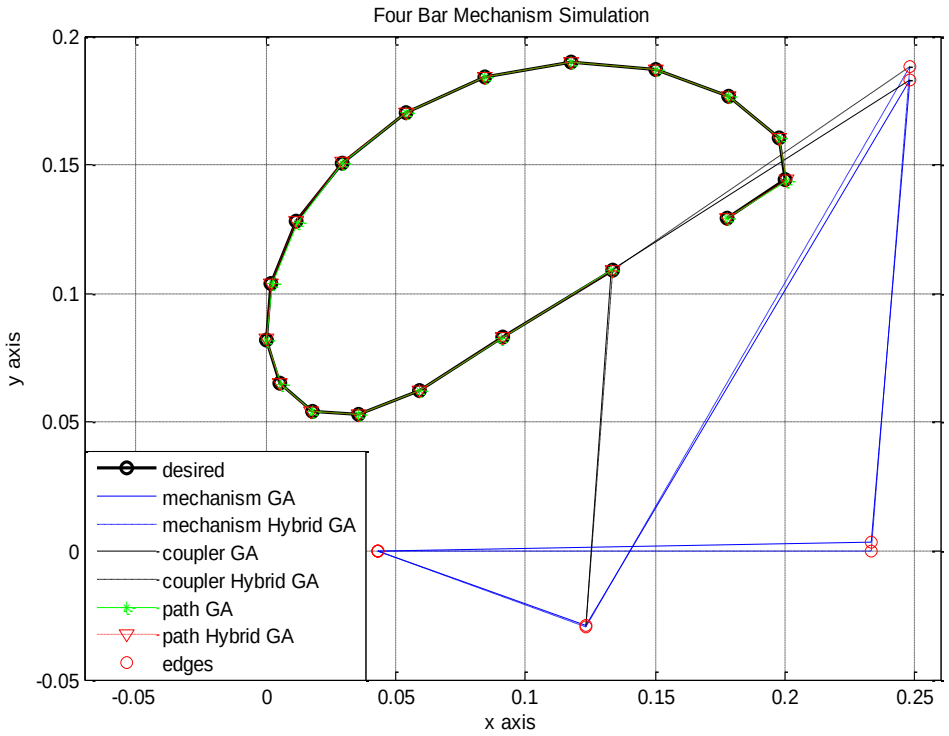

Figure 34: Four-bar Synthesis

4.2.2 Dynamics.

The mechanism design obtained from the previous section is used and the links' shape and volume are to be designed and the motor-gearbox combination selected. Running the optimization so as to minimize the input voltage and the voltage variation by varying the inertia, motors, and gear ratio, the Pareto front is shown in Figure 35.

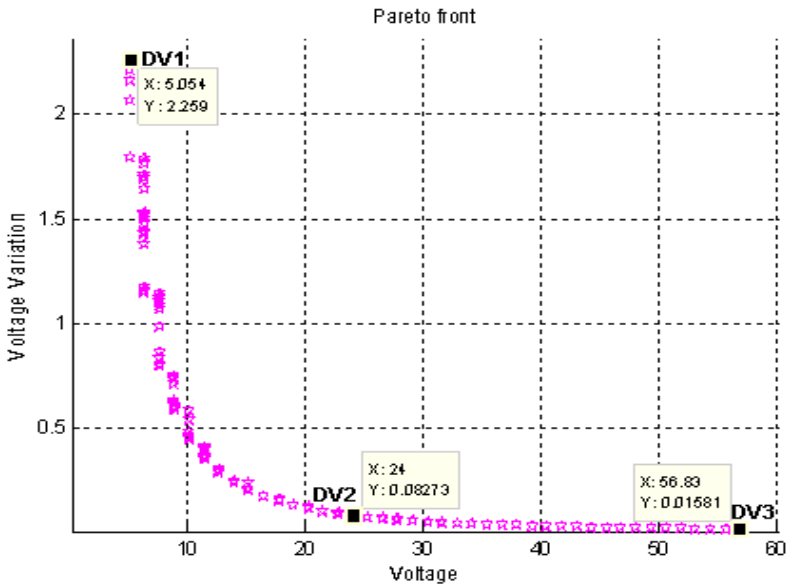

Figure 35: Design Dynamics Pareto Front

The Pareto front provides a set of solutions to be chosen from. The tradeoff between voltage and voltage variation can be observed and the designer can choose what best suites the application. Out of these solutions three designs labeled DV1, DV2 and DV3 are computed and the resulting design vectors are shown in Table 17, Table 18, and Table 19.

Table 17: Dynamics Mechanism Parameters

Mechanism parameters											
DV	(m)	b_i	c_i	d_i	e_i	f_i	g_i	h_i	i_i	j_i	k_i
1	L_2	0.0649	0.0710	0.0623	0.0160	0.0203	0.0604	0.0789	0.0239	0.0361	0.0492
	L_3	0.0999	0.0301	0.0470	0.0061	0.0001	0.0000	0.0077	0.0798	0.0751	0.0981
	L_4	0.0272	0.0302	0.0152	0.0060	0.0000	0.0001	0.0662	0.0932	0.0924	0.0534
2	L_2	0.0605	0.0721	0.0841	0.0149	0.0529	0.0616	0.0793	0.0634	0.0911	0.0676
	L_3	0.1000	0.0302	0.0151	0.0060	0.0001	0.0000	0.0391	0.0156	0.0279	0.0611
	L_4	0.0183	0.0301	0.0153	0.0060	0.0003	0.0002	0.0697	0.0779	0.0735	0.0676
3	L_2	0.0954	0.0863	0.0838	0.0154	0.0436	0.0367	0.0444	0.0910	0.0744	0.0559
	L_3	0.0614	0.0318	0.0161	0.0061	0.0010	0.0003	0.0535	0.0738	0.0402	0.0978
	L_4	0.0310	0.0315	0.0155	0.0060	0.0025	0.0005	0.0826	0.0946	0.0637	0.0964

Table 18: Dynamics Mechanism Inertia Parameters

Mechanism inertia parameters					
DV	(m)	Center of mass location		Mass and inertia	
		r_i (m)	δ_i angle	mass (kg)	J (kg m^2)
1	L_2	0.0443	-0.3978	1.2652	0.0061
	L_3	0.0994	0.0005	0.1960	0.0026
	L_4	0.0738	-0.0004	0.1421	0.0007
2	L_2	0.0556	-0.0406	1.4066	0.0078
	L_3	0.0833	0.0006	0.1778	0.0020
	L_4	0.0770	0.0003	0.1383	0.0007
3	L_2	0.0349	0.0733	1.6404	0.0112
	L_3	0.1031	0.0028	0.1758	0.0016
	L_4	0.0735	0.0069	0.1560	0.0008

Table 19: Dynamics Motor Parameters

Motor parameters								
DV	M#	R (Ω)	L (H)	km (Nm/A)	kg (Vs)	J (kg m^2)	B (Nms)	n
1	11	0.24	0.31e-3	0.042	0.042	4.73e-5	1.68e-5	4
2	11	0.24	0.31e-3	0.042	0.042	4.73e-5	1.68e-5	19
3	11	0.24	0.31e-3	0.042	0.042	4.73e-5	1.68e-5	45

The second design vector is designed on inventor and is shown in Figure 36 for visualization.

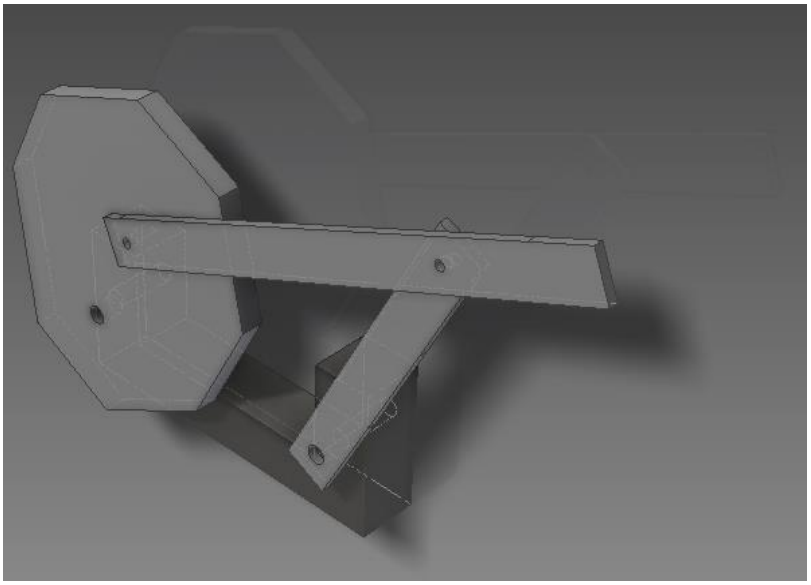

Figure 36: Designed Mechanism DV2

The voltage fluctuation required for running the mechanism at a constant speed of 30 rad/s is computed and the mean voltage is given to the mechanism to see the effect on the crank angular speed response. This is evaluated for the three design vectors as shown in Figure 37 and Figure 38.

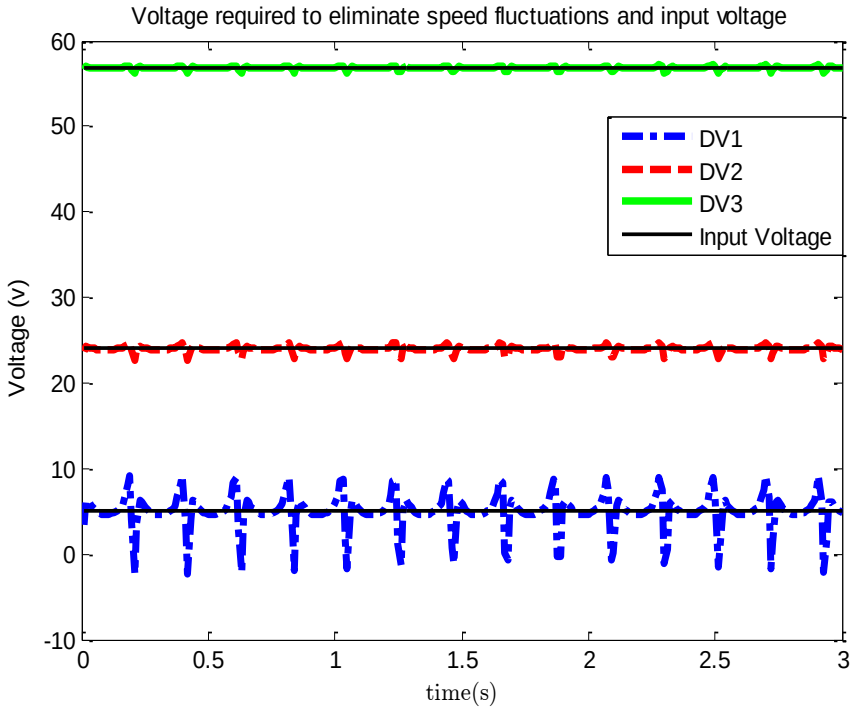

Figure 37: Sequential Design Vectors Voltage Fluctuation and Input Voltage

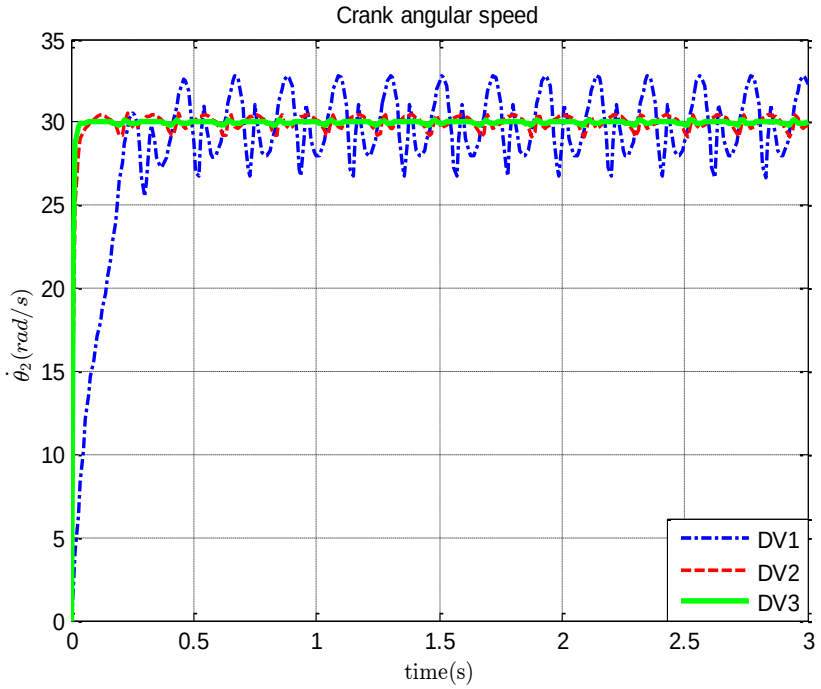

Figure 38: Sequential Design Vectors Crank Angular Speed Response

A detailed analysis is carried out for DV2 in steady state. The current, torque, and the loss decomposition are shown in Figure 39, Figure 40, and Figure 41, respectively.

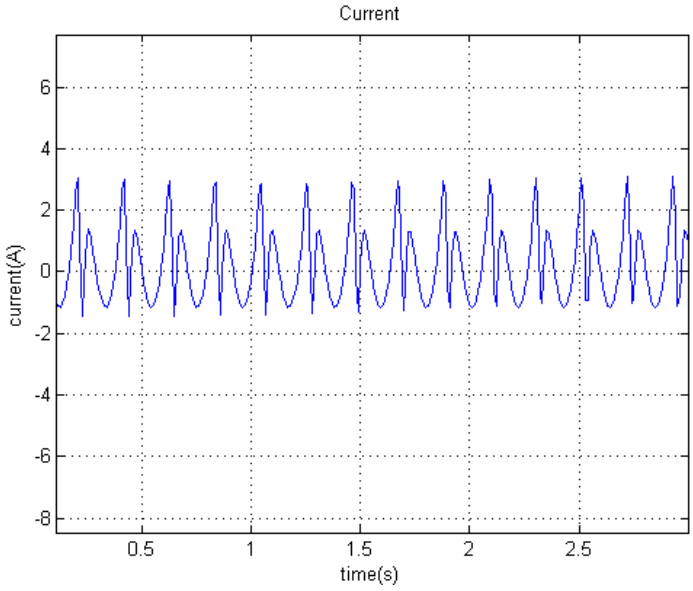

Figure 39: DV2 Current

The current required to run the mechanism at 30 rad/s for design vector 2 varies between -1 and 3, whereas the motor's continuous torque current specification is 9.98 A.

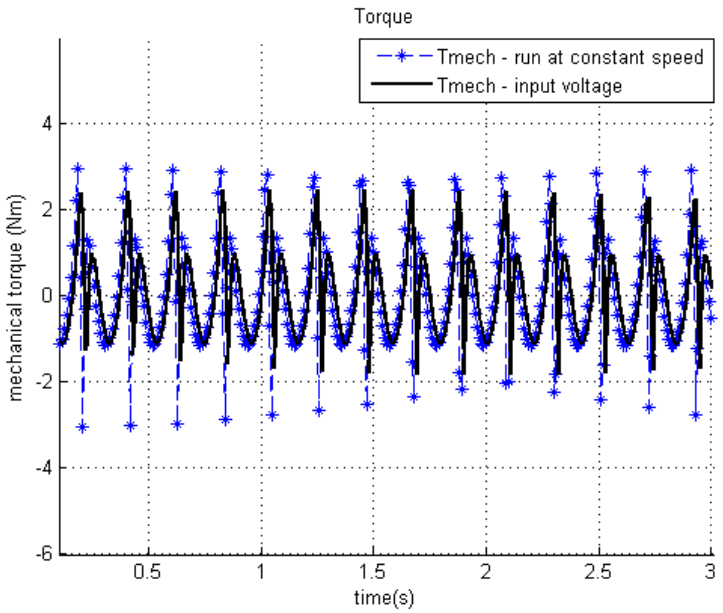

Figure 40: DV2 Required Torque and Delivered

The torque required for running at a constant speed of 30 rad/s is shown above along with the torque response of DV2. The small variations are due to fact that the DV2 speed response is fluctuating around 30 rad/s.

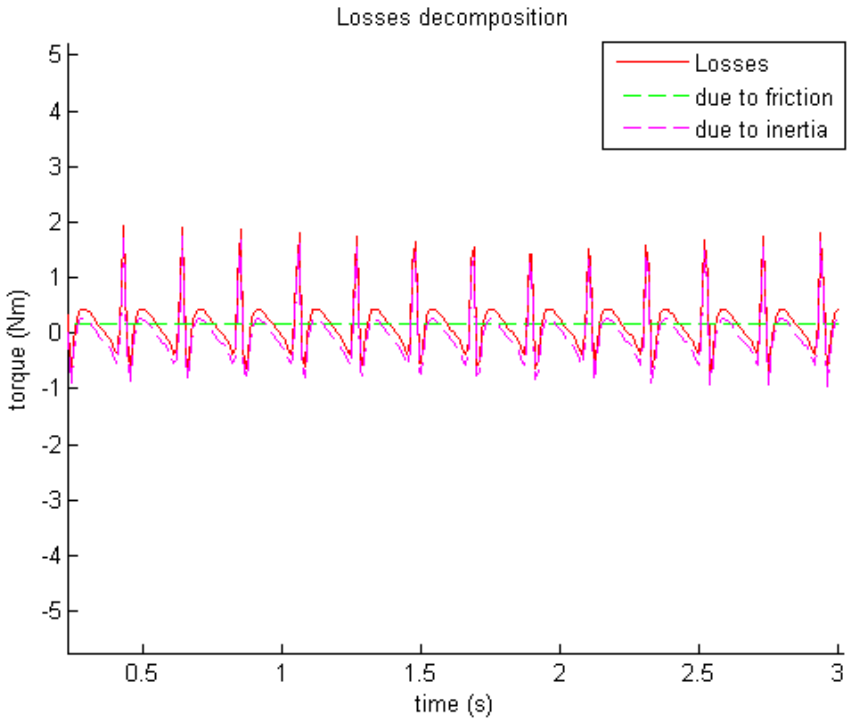

Figure 41: DV2 Losses Decomposition

It can be seen that the mechanical loss is mainly inertial and the viscous friction loss is small. The inertial loss will be eliminated when running at a constant speed.

4.2.3 Control.

The mechanical and electronic designs are fixed and a control system is to be designed to meet certain system specifications. It is desired that the system's speed response has a rise time of 0.01 s, an overshoot of 0.5 %, and a steady state error of 0.1 %. The three design vectors selected in the previous section are going to be considered for control. A modified PID controller is implemented for the design vectors and the results are shown in Figure 42 and Table 20.

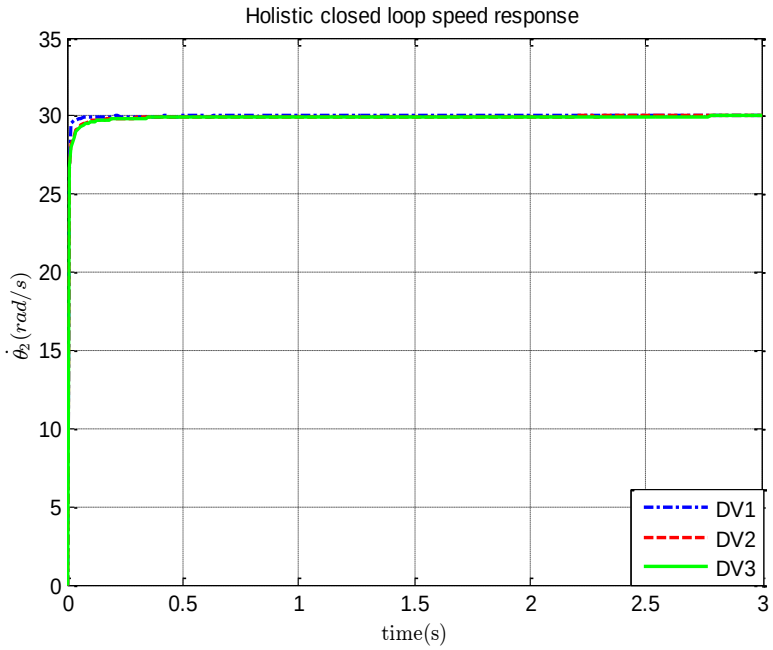

Figure 42: PID Closed-Loop Speed Response

Table 20: PID Control Gains and Specifications

DV	Specifications			Gains		
	Rise time (s)	Overshoot (%)	S.S.E (%)	K_p	K_i	K_d
1	0.0079	0.50	0.1	53.7	0.126	0.00824
2	0.0084	-1.03	0.1	34.1	0.504	7e-7
3	0.0090	-1.06	0.1	55.8	0.289	1e-7

It can be observed that the differential gain is negligible as the open loop response has less fluctuations. Hence, a modified PI controller is going to be implemented instead. The modified PI controller was implemented in [16] and is represented by the control law in (142).

$$u(t) = K_p e(t) \int_0^t \dot{\theta}_2^d dt + K_i \int_0^t e(t) dt \tag{142}$$

The controller is implemented on the three design vectors and the results are shown in Figure 43 and Table 21.

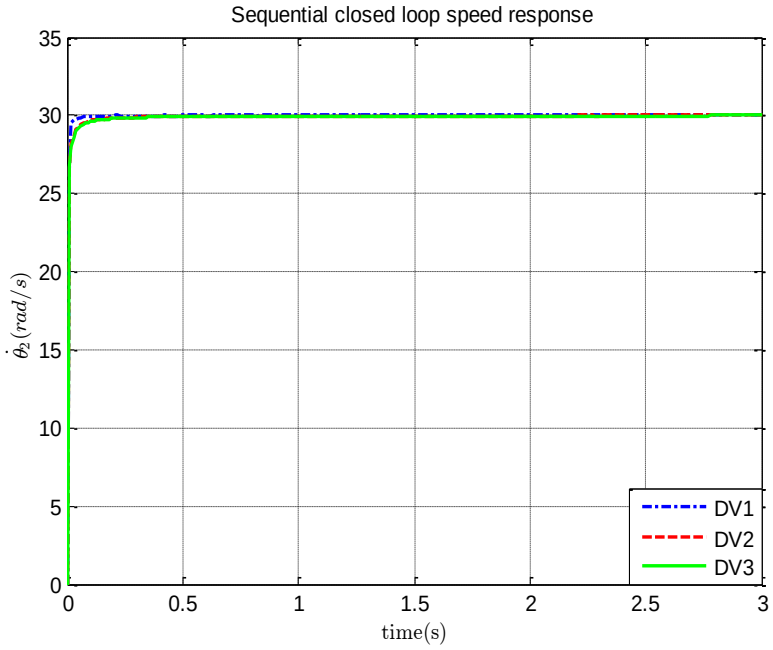

Figure 43: PI Closed-Loop Speed Response

Table 21: PI Control Gains and Specifications

DV	Specifications			Gains	
	Rise time (s)	Overshoot (%)	S.S.E (%)	K_p	K_i
1	0.010	-0.260	0.1	23.5	1.50
2	0.010	-1.19	0.1	17.6	17.9
3	0.010	-1.17	0.1	43.8	9.62

A detailed analysis is carried out for DV2 in the open and closed loop. The current, current rate, angular position, and acceleration are shown in Figure 44.

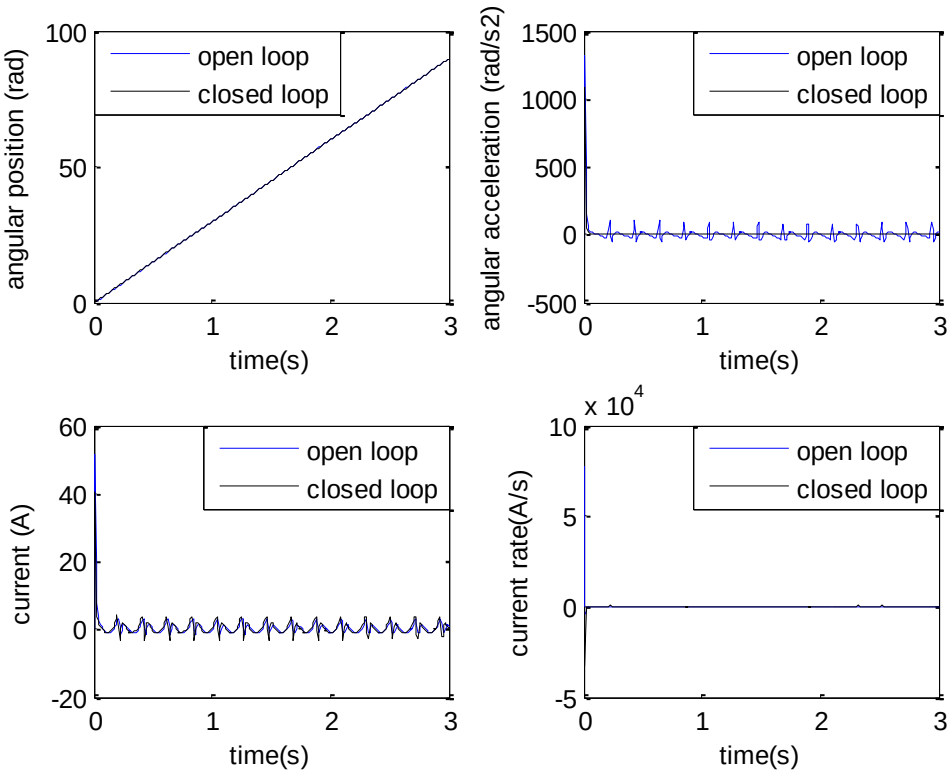

Figure 44: DV2 Open-Loop and Closed-Loop Behavior

4.3 Holistic Approach

The holistic design methodology is going to be represented in this section, where all the system variables are designed simultaneously. The design vector is presented in equation (143).

$$X = [\, x_0,\ y_0, \theta_1,\ L_i,\ r_{cx}, r_{cy}, \theta_2\ ,\ b_{\mathrm{i}},\ c_{\mathrm{i}}, d_{\mathrm{i}},\ e_i,\ f_i, g_i, h_{\mathrm{i}},\ i_{\mathrm{i}}, j_{\mathrm{i}}, k_i,\ M_{\#}, \mathrm{n}, K_p, K_i] \quad (143)$$

The design vector is made of 45 variables. The first 10 variables are for synthesis, and then 30 variables are for the volume of the links, 1 variable is for the motor index, 1 variable is for the gear ratio, and the last 2 variables are for the control gains.

The genetic algorithm is used to minimize the four objectives by searching the design space. The objectives to be minimized are the path error, voltage, voltage variation, and the proportional control gain. The objectives are given by (144-147).

$$\mathrm{f}_1\colon \min\Big(\sum_{i=1}^{n}\big(C_{xd}^{i} - C_{xr}^{i}\big)^2 + \big(C_{yd}^{i} - C_{yr}^{i}\big)^2\Big)^{1/2} \quad (144)$$

$$\mathrm{f}_2\colon \min(V + m_1 \times C_1 + m_2 \times C_2 + m_3 \times C_3) \quad (145)$$

$$f_3: \min\left(\frac{V_{max} - V_{min}}{V_{avg}}\right) \tag{146}$$

$$f_4: \min\left(K_p + m_4 \times C_4 + m_5 \times C_5 + m_6 \times C_6\right) \tag{147}$$

where C_d^i represents the desired points to track, C_r^i represents the generated coupler points, V is the input voltage, $C_1, C_2, C_3, C_4, C_5$and, C_6 are constraints to be met by the optimization problem, and m_i is a high-value number that penalizes the objective function if the constraint is not met.

The optimization problem yields a set of non-dominated solutions, called the Pareto front, which the designer can choose from for his application. The Pareto front of the optimization problem is shown in Figure 45.

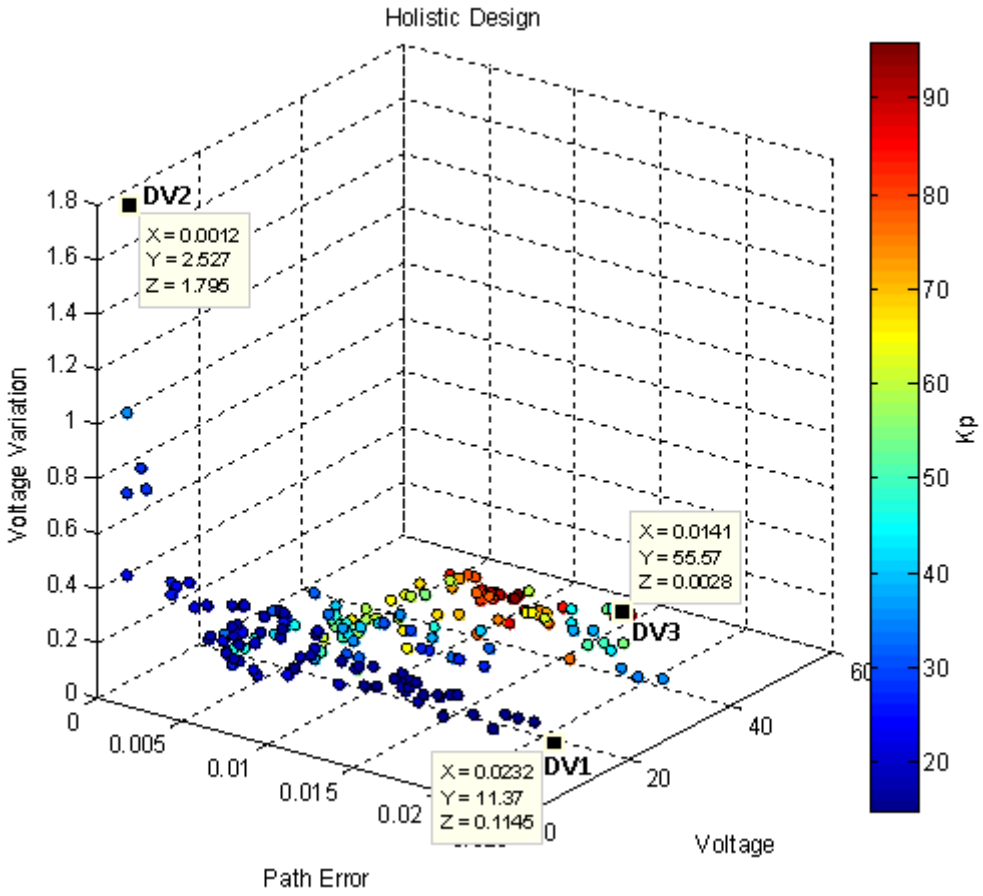

Figure 45: Holistic Design Pareto Front

Out of these solutions, three designs labeled DV1, DV2, and DV3 are computed and the resulting design vectors and inertia parameters are shown in Table 22, Table 23, Table 24, and Table 25.

Table 22: Holistic Design Mechanism Parameters

Mechanism parameters												
DV	(m)	l_i	b_i	c_i	d_i	e_i	f_i	g_i	h_i	i_i	j_i	k_i
1	L_1	0.1853										
	L_2	0.0834	0.0269	0.0863	0.0533	0.0187	0.0205	0.0623	0.0987	0.0453	0.0794	0.0507
	L_3	0.2535	0.1000	0.0339	0.0330	0.0073	0.0128	0.0009	0.0342	0.0677	0.0898	0.0908
	L_4	0.1925	0.0187	0.0303	0.0174	0.0061	0.0157	0.0010	0.0846	0.0924	0.0752	0.0757
2	L_1	0.1893										
	L_2	0.0850	0.0691	0.0721	0.0611	0.0169	0.0147	0.0603	0.0739	0.0272	0.0397	0.0498
	L_3	0.2500	0.0989	0.0317	0.0416	0.0061	0.0004	0.0003	0.0074	0.0834	0.0607	0.0948
	L_4	0.1886	0.0195	0.0322	0.0170	0.0063	0.0006	0.0003	0.0623	0.0888	0.0889	0.0524
3	L_1	0.1835										
	L_2	0.0801	0.0592	0.0882	0.0866	0.0297	0.0631	0.0153	0.0567	0.0614	0.0491	0.0240
	L_3	0.2615	0.0884	0.0322	0.0176	0.0062	0.0006	0.0039	0.0632	0.0509	0.0254	0.0612
	L_4	0.1935	0.0566	0.0324	0.0184	0.0070	0.0036	0.0021	0.0782	0.0963	0.0456	0.0950

Table 23: Holistic Design Mechanism Inertia Parameters

Mechanism inertia parameters					
DV	(m)	Center of mass location		Mass and inertia	
		r_i (m)	δ_i angle	mass (kg)	J (kg m^2)
1	L_2	0.0580	-0.2445	1.1501	0.0041
	L_3	0.0577	0.0910	0.2829	0.0023
	L_4	0.0833	0.0488	0.1822	0.0009
2	L_2	0.0426	-0.4656	1.3166	0.0064
	L_3	0.0661	0.0012	0.1745	0.0016
	L_4	0.0790	0.0008	0.1542	0.0008
3	L_2	0.0565	0.3259	2.7105	0.0153
	L_3	0.0559	-0.0260	0.1728	0.0012
	L_4	0.0692	0.0056	0.2145	0.0013

Table 24: Holistic Design Motor Parameters

Motor parameters								
DV	M#	R (Ω)	L (H)	km (Nm/A)	kg (Vs)	J (kg m^2)	B (Nms)	n
1	11	0.24	0.31e-3	0.042	0.042	4.73e-5	1.68e-5	9
2	11	0.24	0.31e-3	0.042	0.042	4.73e-5	1.68e-5	2
3	11	0.24	0.31e-3	0.042	0.042	4.73e-5	1.68e-5	44

Table 25: Holistic Design Control Parameters

Control parameters					
DV	Specifications			Gains	
	Rise time (s)	Overshoot (%)	S.S.E (%)	K_p	K_i
1	0.0099	-0.844	0.1	14.9	2.89
2	0.0099	0.170	0.1	42.1	0.682
3	0.0087	-0.796	0.1	90.8	9.98

The generated path is evaluated for the three design vector mechanisms in Figure 46 and compared with the result obtained in the sequential design.

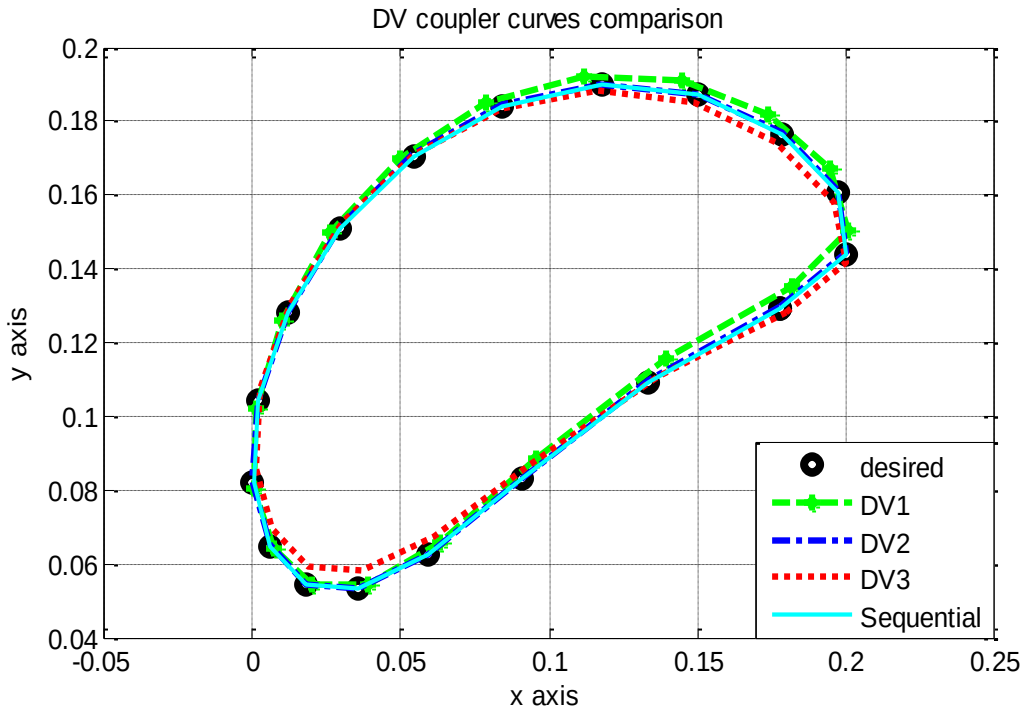

Figure 46: Designed Coupler Curves Comparison

It can be observed that the mechanism obtained in the sequential design and DV2 follow the desired path more accurately than DV1 and DV3. However, this slight offset will help obtain better results in the other objective functions which will be shown later. The mechanisms obtained from the three design vectors are superimposed in Figure 47 for visualization.

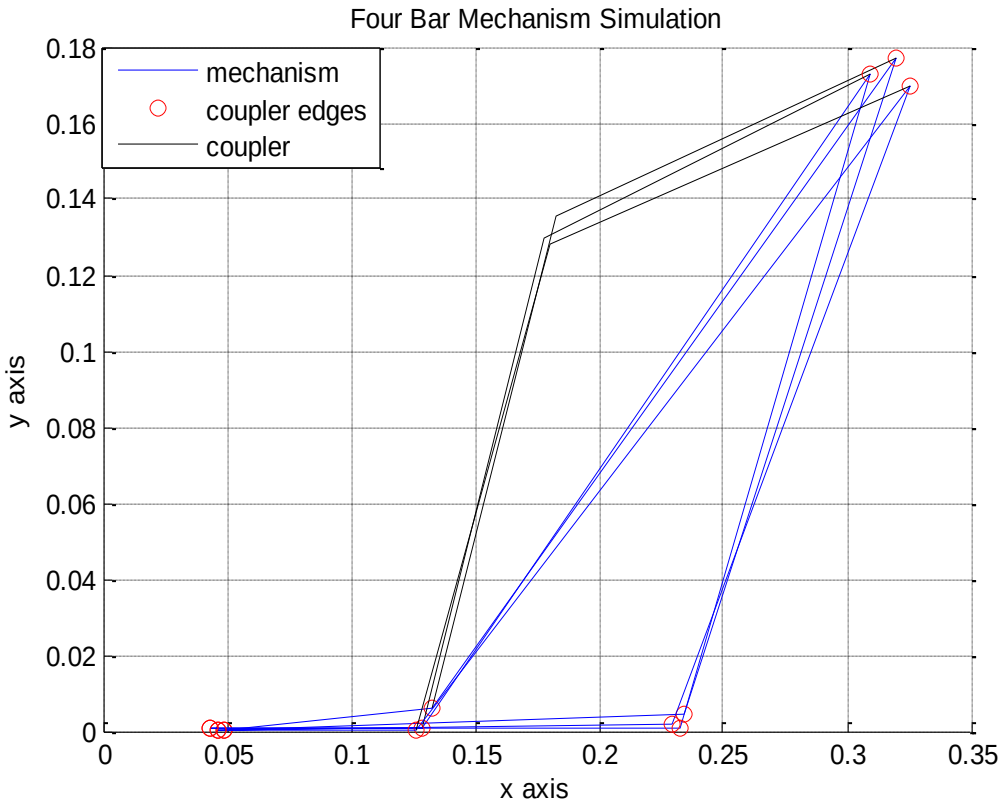

Figure 47: DV1, DV2, and DV3 Mechanisms

The mechanism obtained from the first design vector is designed on inventor and is shown in Figure 48 for visualization.

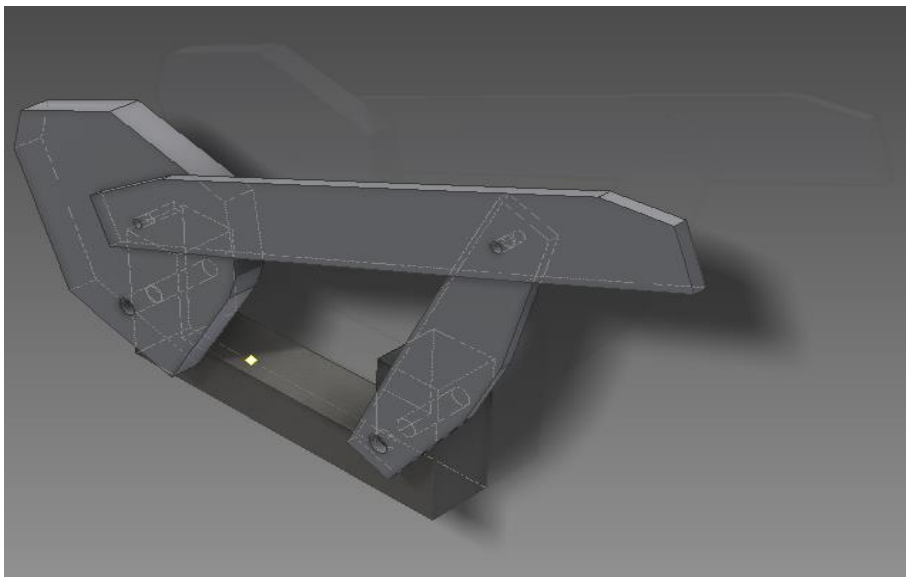

Figure 48: Designed Mechanism DV1

The voltage fluctuation required for running the mechanism at a constant speed of 30 rad/s is computed and the mean voltage is given to the mechanism to see

the effect on the crank angular speed response. This is evaluated for the three design vectors and is shown in Figure 49 and Figure 50.

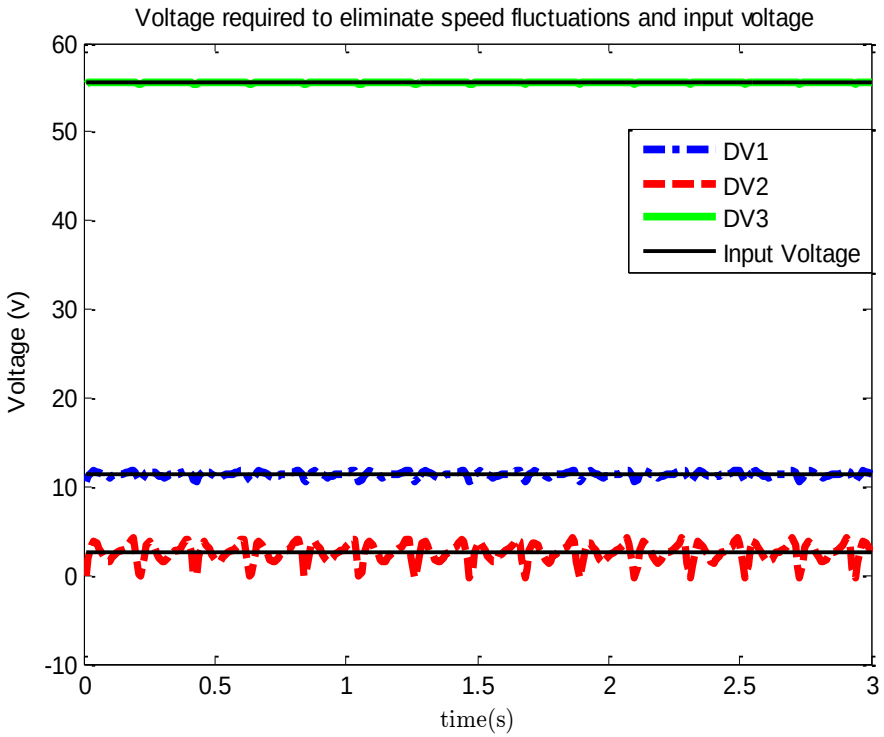

Figure 49: Holistic Design Vectors Voltage Fluctuation and Input Voltage

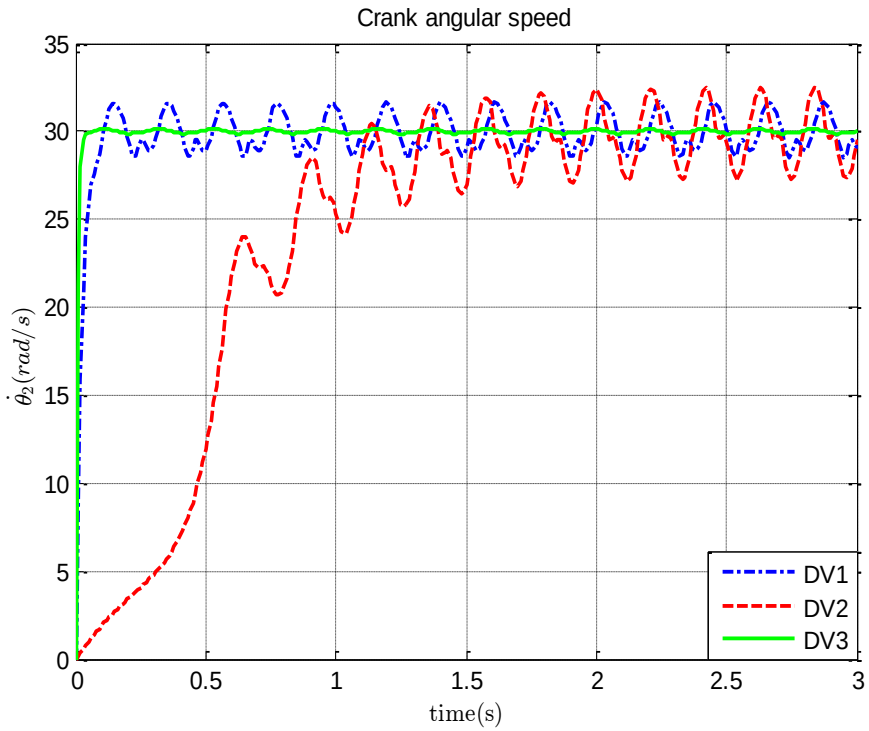

Figure 50: Holistic Design Vectors Crank Angular Speed Response

4.4 Design Comparison

The solution that had the highest voltage variation from the sequential design is compared to the solution with the highest voltage variation in the holistic design Pareto front and the results are shown in Figure 51.

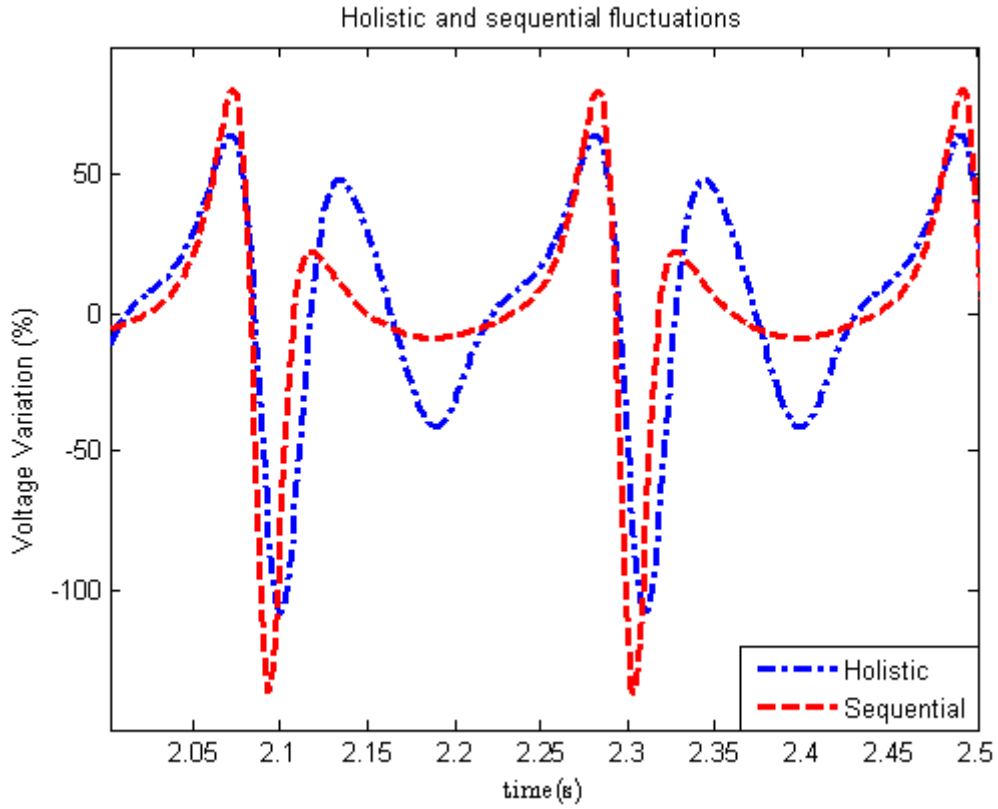

Figure 51: Highest Voltage Variation Comparison

It can be noticed that the holistic design solution has less variation than the sequential design. It can be observed from the Pareto fronts that the maximum voltage variation decreased from 2.259 to 1.79 in the holistic design. This is due to the fact that the mechanism links and the dynamics are varying together. It can also be observed from Figure 52 that the minimum input voltage to run the mechanism decreased from 5.054 to 2.527 volts in the holistic design for the same reason. The average voltage is given to both mechanisms and the crank angular speed response is shown in Figure 53.

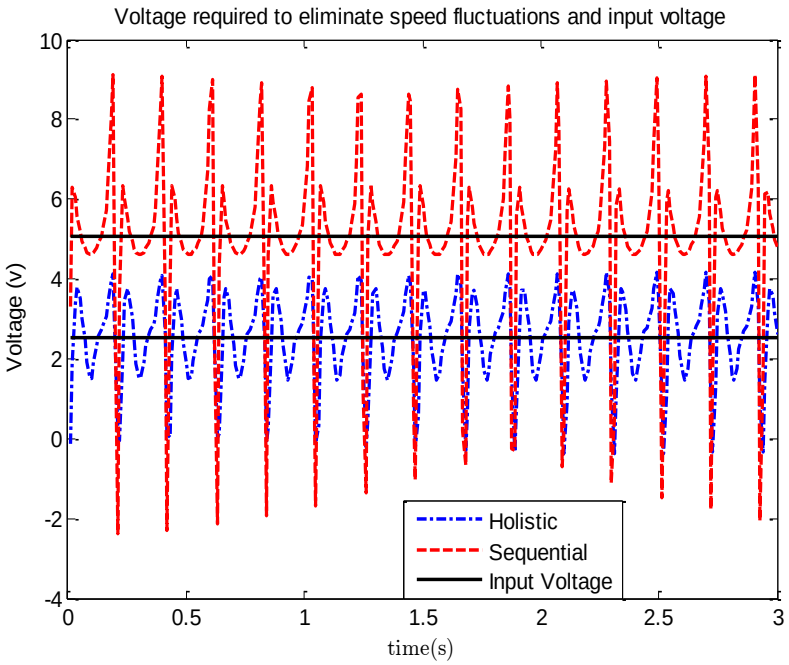

Figure 52: Holistic DV2 and Sequential DV1 Voltage Variation and Input Voltage Comparison

The angular speed fluctuations are smaller for the holistic solution than for the sequential.

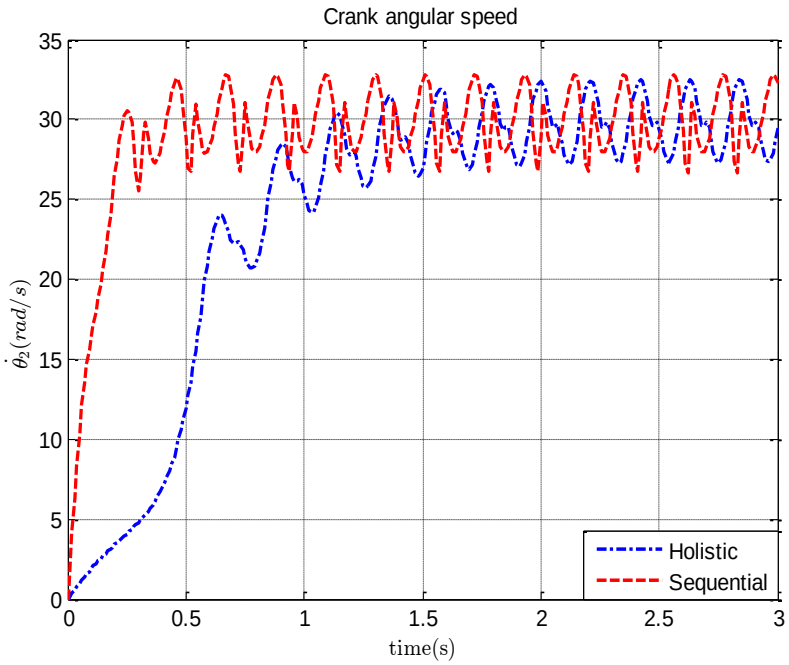

Figure 53: Holistic DV2 and Sequential DV1 Speed Response Comparison

The solution that had the lowest voltage variation from the sequential design is compared to the solution with the lowest voltage variation in the holistic design Pareto front and the results are shown in Figure 54.

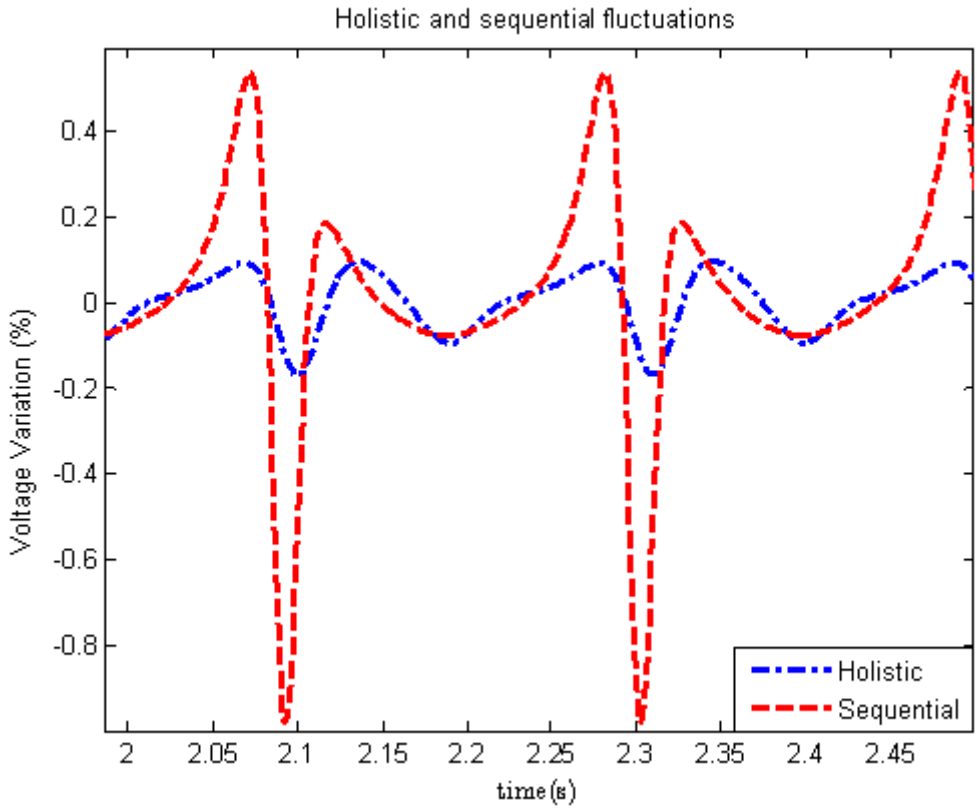

Figure 54: Lowest Voltage Variation Comparison

It can be noticed that the holistic design solution has less voltage variation than the sequential design. It can be observed from the Pareto fronts that the minimum voltage variation decreased from 0.0158 to 0.0028 in the holistic design. This is due to the fact that the mechanism's geometric parameters and dynamics are considered simultaneously. It can also be observed from Figure 55 that the maximum input voltage to run the mechanism decreased from 56.83 to 55.57 volts in the holistic design for the same reason.

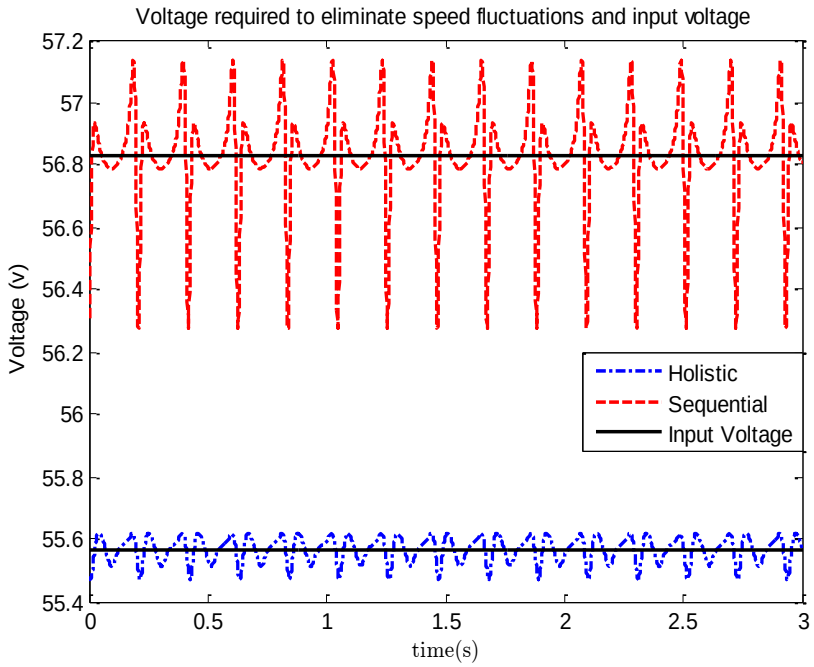

Figure 55: Holistic DV3 and Sequential DV3 Voltage Variation and Input Voltage Comparison

The average voltage is given to both mechanisms and the crank angular speed response is shown in Figure 56.

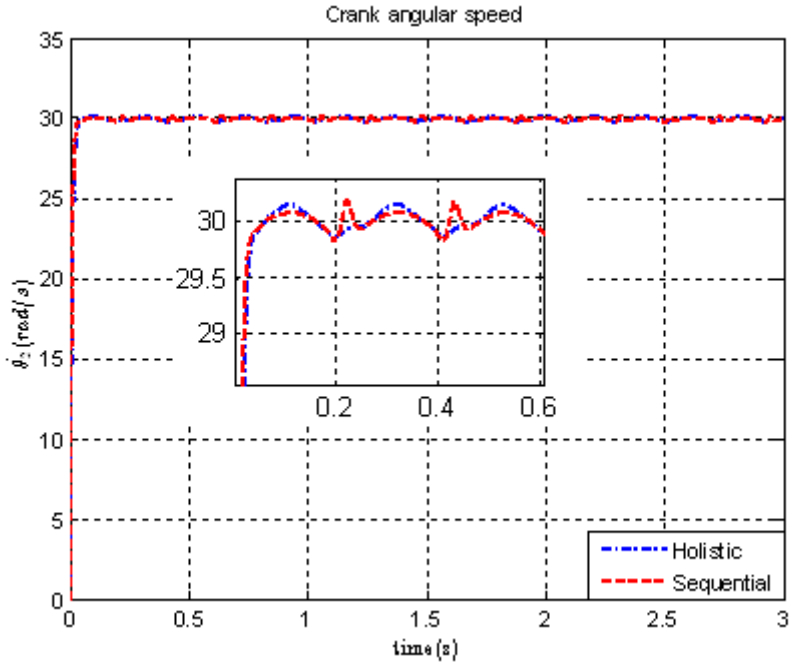

Figure 56: Holistic DV3 and Sequential DV3 Speed Response Comparison

The closed-loop response of the three selected design vectors is shown in Figure 57.

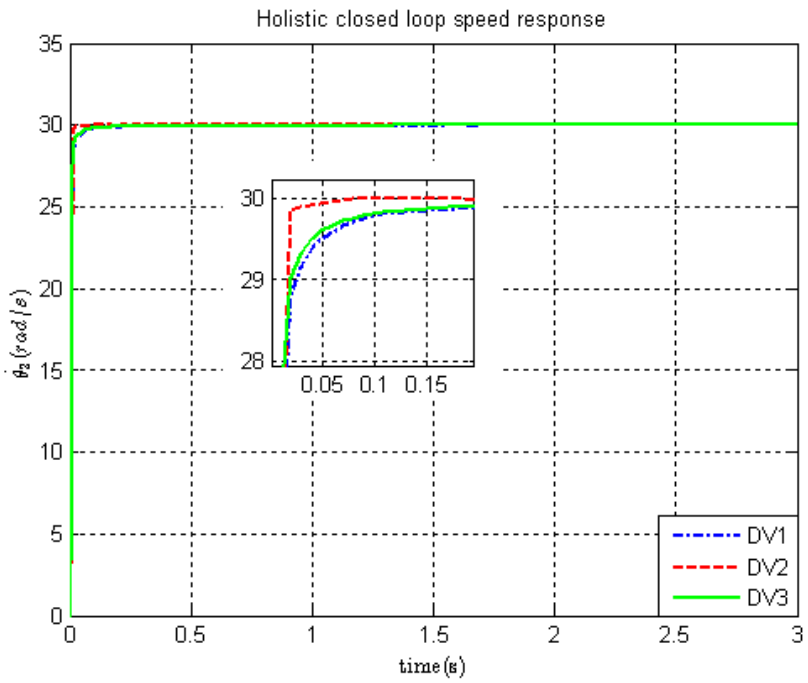

Figure 57: Holistic Closed-Loop Response

The solution that had the lowest gain from the sequential design is compared to the solution with the lowest gain in the holistic design Pareto front and the results are shown in Table 26.

Table 26: Control Gains Comparison

	Specifications			Gains	
	Rise time (s)	Overshoot (%)	S.S.E (%)	K_p	K_i
Holistic	0.0099	-0.844	0.1	14.9	2.90
Sequential	0.0100	-1.19	0.1	17.6	17.9

The holistic solution has smaller gains than the sequential one due to the fact that the open-loop system is not fixed and is changing with the controller.

The open-loop and the closed -loop response of the two solutions are shown in Figure 58 and Figure 59.

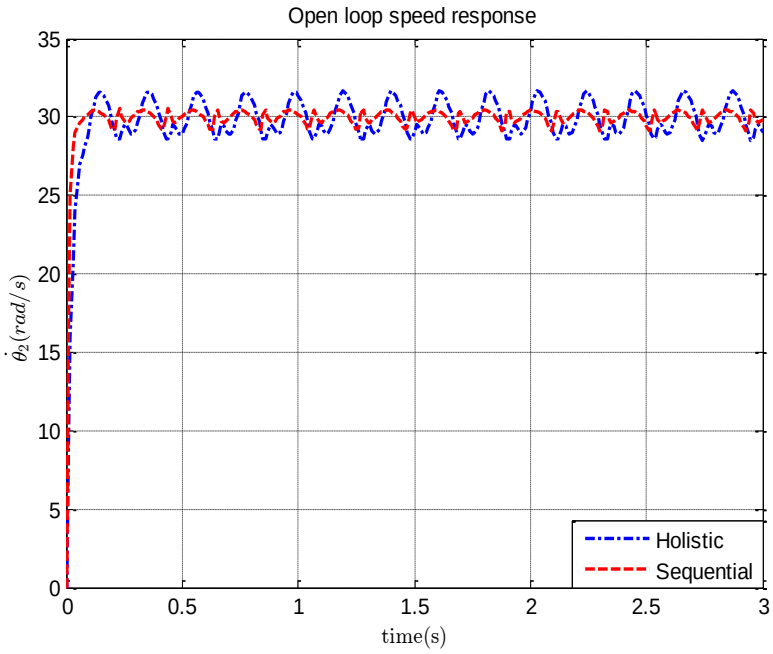

Figure 58: Open-Loop Response Comparison

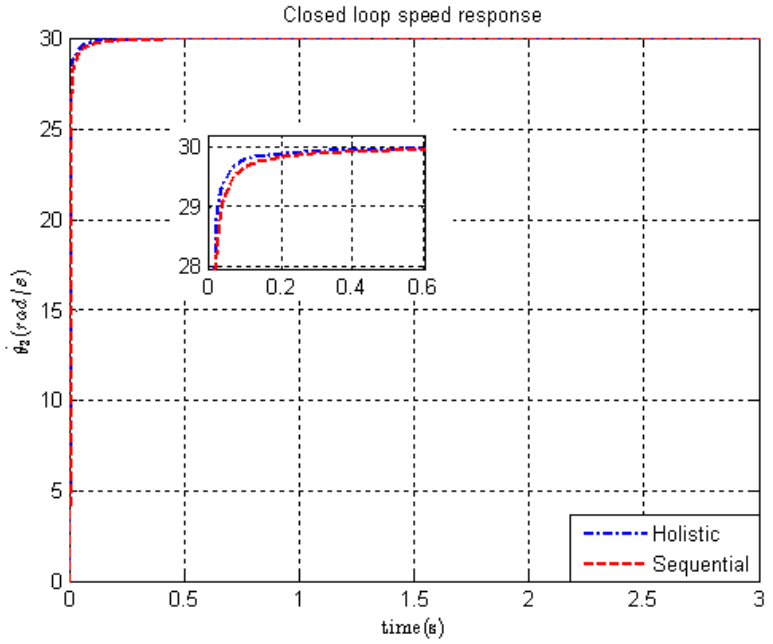

Figure 59: Closed-Loop Response Comparison

In terms of computational time, the sequential approach took around 1 day to compute the results while the holistic approach took from 2 to 3 days. A population of 500 and 500 generations of evolution are used to run the GA for both design approaches. The processor used is an Intel Core 2 Quad. To reduce the computational time, a faster processor can be used and parallel computing as well can reduce the computational time significantly. Genetic algorithm was used to provide a set of non-

dominated solutions of the whole system to the designer and by allowing all the variables to change simultaneously better solutions than the sequential approach can be obtained. The differences between the designs in open loop, in terms of voltage and voltage variation, are quite significant. In closed loop the improvement is small. The algorithm can do further minimization of the objective functions if the tolerance of error in path following, when designing the geometry of the mechanism, is increased.

Chapter 5: Conclusion and Future Work

5.1 Conclusion

In this research, a holistic design methodology of mechatronic systems was proposed. The design methodology uses heuristic optimization techniques to design the mechanical, electronic, and control systems simultaneously. The optimization problem designs the system geometry, inertia parameters, motor-gearbox combination selection, and control gains. It also provides a set of non-dominated design solutions called a "Pareto front" from which the designer can choose the design that best suites his application. The sequential design methodology was first presented, where the geometry was optimized and fixed; then the dynamic behavior of the system was optimized considering a set of motors and gearbox combinations along with the system inertia, and then a control system was optimized based on the previously-obtained system. The holistic design methodology was then presented, where all these variables are designed simultaneously. The design methodologies were applied to a four-bar mechanism driven by a DC motor. The objective functions to be minimized are the tracking path error for geometry design, the input voltage and voltage fluctuations to run at a desired speed for the dynamics design, and the proportional gain for the control design. The two design methodologies were compared and it was shown that the holistic design approach provided some solutions that have smaller voltage, voltage variation, and control effort than the sequential approach. This is due to the fact that in the holistic approach the geometry, dynamics, and control are considered simultaneously. Hence, at the expense of having slightly more path tracking error in geometry design, a better dynamic behavior can be achieved. Also, by varying the coupled system parameters, a controller with less control effort can be achieved.

5.2 Future Work

A proposed scope of future work might focus on hardware implementation of one of the obtained design solutions or implementing the proposed holistic design methodology on other dynamic systems such as a quadrotor. The work on four-bar mechanisms can be extended to consider the choice of materials, balancing the shaking moment and forces, or working in the non-dimensional domain. The work can also be extended and implemented to other mechanisms or the problem can be

solved using other heuristic optimization techniques. It is also possible to design a system with the purpose of further understanding the interconnection between different disciplines of the system through holistic design.

References

[1] A. Alvarez Cabrera, M. Foeken, O. Tekin, K. Woestenenk, M. Erden, B. De Schutter, M. van Tooren, R. Babuška, F. van Houten and T. Tomiyama, "Towards automation of control software: A review of challenges in mechatronic design", *Mechatronics*, vol. 20, no. 8, pp. 876-886, 2010.

[2] R. Chhabra and M. Reza Emami, "Holistic system modeling in mechatronics", *Mechatronics*, vol. 21, no. 1, pp. 166-175, 2011.

[3] Y. Wang, Y. Yu, C. Xie, X. Zhang and W. Jiang, "A proposed approach to mechatronics design education: Integrating design methodology, simulation with projects", *Mechatronics*, vol. 23, no. 8, pp. 942-948, 2013.

[4] S. Acharyya and M. Mandal, "Performance of EAs for four-bar linkage synthesis", *Mechanism and Machine Theory*, vol. 44, no. 9, pp. 1784-1794, 2009.

[5] W. Lin, "A GA–DE hybrid evolutionary algorithm for path synthesis of four-bar linkage", *Mechanism and Machine Theory*, vol. 45, no. 8, pp. 1096-1107, 2010.

[6] A. Smaili, N. Atallah, and F. Zeineddine, "OptimaLink: A MATLAB-based code for teaching/learning precision-point and optimum synthesis and simulation of mechanisms", *Int J Engineering Education*, vol. 21, no. 5, pp. 874-884, 2005.

[7] B. EL-Kribi, A. Houidi, Z. Affi and L. Romdhane, "Application of multi-objective genetic algorithms to the mechatronic design of a four-bar system with continuous and discrete variables", *Mechanism and Machine Theory*, vol. 61, pp. 68-83, 2013.

[8] Z. Affi, B. EL-Kribi and L. Romdhane, "Advanced mechatronic design using a multi-objective genetic algorithm optimization of a motor-driven four-bar system", *Mechatronics*, vol. 17, no. 9, pp. 489-500, 2007.

[9] M. B. Calva-Yáñez, P. A. Niño-Suárez, M. G. Villarreal-Cervantes, G. Sepúlveda-Cervantes, and E. A. Portilla-Flores, "Differential Evolution for the Control Gain's Optimal Tuning of a Four-bar Mechanism", *Polibits*, vol. 47, pp. 67-73, 2013.

[10] G. Renner and A. Ekárt, "Genetic algorithms in computer aided design", *Computer-Aided Design*, vol. 35, no. 8, pp. 709-726, 2003.

[11] Daerospace.com, "Four Bar Linkage - Description", 2015. [Online]. Available: http://www.daerospace.com/MechanicalSystems/FourBarLinkageDesc.php. [Accessed: 10- May- 2015].

[12] A. Y., R. J. Romero-Troncoso, L. Morales-Velazquez and R. A., "PID-Controller Tuning Optimization with Genetic Algorithms in Servo Systems", *Int J Advanced Robotic Systems*, vol. 10, pp. 324-338, 2013.

[13] R. Haupt, S. Haupt and R. Haupt, *Practical genetic algorithms*. Hoboken, N.J.: John Wiley, 2004.

[14] MIT open courseware, "13. Learning: Genetic Algorithms", 2015. [Online]. Available:https://www.youtube.com/watch?v=kHyNqSnzP8Y&list=PLUl4u3cNGP63gFHB6xb-kVBiQHYe_4hSi&index=13. [Accessed: 05- May- 2015].

[15] R. Norton, *Kinematics and dynamics of machinery*. Boston, Mass.: McGraw-Hill, 2009.

[16] G. Sandor and A. Erdman, *Advanced mechanism design*. Englewood Cliffs/N.J: Prentice-Hall, 1984.

[17] N. Nariman-Zadeh, M. Felezi, A. Jamali and M. Ganji, "Pareto optimal synthesis of four-bar mechanisms for path generation", Mechanism and Machine Theory, vol. 44, no. 1, pp. 180-191, 2009.

[18] J. Shigley and J. Uicker, *Theory of machines and mechanisms*. New York: McGraw-Hill, 1980.

[19] F. Raven, "Position, velocity, and acceleration analysis and kinematic synthesis of plane and space mechanisms by a generalized procedure called the method of independent position equations," Ph.D. Thesis, Cornell University, [Ithaca, N.Y.], 1958.

[20] Mathworks.com, "Genetic Algorithm - MATLAB", 2014. [Online]. Available: http://www.mathworks.com/discovery/genetic-algorithm.html. [Accessed: 01- Sep- 2014].

[21] J. E. Baker, "Reducing bias and inefficiency in the selection algorithm", In Proc. of the Second International Conference on Genetic Algorithms, pp. 14-21, 1987.

[22] M. Kalos and P. Whitlock, *Monte Carlo methods*. Weinheim: Wiley-Blackwell, 2008.

[23] J. Cabrera, A. Simon and M. Prado, "Optimal synthesis of mechanisms with genetic algorithms", Mechanism and Machine Theory, vol. 37, no. 10, pp. 1165-1177, 2002.

[24] A. Kunjur, and S. Krishnamurty, "Genetic algorithms in mechanical synthesis", Journal of Applied Mechanisms and Robotics, vol. 4, no.2, pp. 18–24, 1997.

[25] M. Villarreal-Cervantes, C. Cruz-Villar, J. Alvarez-Gallegos and E. Portilla-Flores, "Robust structure-control design approach for mechatronic systems", IEEE/ASME Trans. Mechatron., vol. 18, no. 5, pp. 1592-1601, 2013.

[26] M. Villarreal-Cervantes, C. Cruz-Villar, J. Alvarez-Gallegos and E. Portilla-Flores, "Differential evolution techniques for the structure-control design of a five-bar parallel robot", Engineering Optimization, vol. 42, no. 6, pp. 535-565, 2010.

[27] R. Hibbeler, *Statics and mechanics of materials*. Upper Saddle River, N.J.: Pearson/Prentice Hall, 2004.

[28] S. Saha, *Introduction to robotics*. New Delhi: Tata McGraw-Hill, 2008.

[29] Pittman-motors.com, "Pittman Brush DC Motors", 2015. [Online]. Available: http://www.pittman-motors.com/Brush-DC-Motors.aspx. [Accessed: 01- Mar- 2015].

[30] H. van de Straete, P. Degezelle, J. De Schutter and R. Belmans, "Servo motor selection criterion for mechatronic applications", IEEE/ASME Trans. Mechatron., vol. 3, no. 1, pp. 43-50, 1998.

[31] F. Roos, H. Johansson and J. Wikander, "Optimal selection of motor and gearhead in mechatronic applications", Mechatronics, vol. 16, no. 1, pp. 63-72, 2006.

[32] N. Nise, *Control systems engineering*. Hoboken, NJ: Wiley, 2011.

[33] R. Dorf and R. Bishop, *Modern control systems*. Upper Saddle River, NJ: Prentice Hall, 2001.

[34] G. Franklin, J. Powell and A. Emami-Naeini, *Feedback control of dynamic systems*. Reading, Mass.: Addison-Wesley, 1994.

[35] J. Tao and J. Sadler, "Constant speed control of a motor driven mechanism system", Mechanism and Machine Theory, vol. 30, no. 5, pp. 737-748, 1995.

Vita

Islam Adel Helmy earned his B.Sc degree in Mechanical Engineering with a minor in Aeronautical Engineering from the *American University of Sharjah* in 2012. He then started his Master of Science program in Mechatronics Engineering. In 2013 he joined *Emirates Airlines* as an engineering repairs coordinator. Islam worked on several academic projects in design such as designing and manufacturing of an unmanned aerial vehicle, and designing a mobile robot.